Impurities and Current Efficiency in Aluminum Electrolysis

Rauan Meirbekova

Doctor of Philosophy

September 2015

School of Science and Engineering

Reykjavík University

Ph.D. Dissertation

ISBN 978-9935-9147-5-0

Impurities and Current efficiency in Aluminum Electrolysis

Dissertation submitted to the School of Science and Engineering
at Reykjavík University in partial
fulfillment of the requirements for the degree
of
Doctor of Philosophy (Ph.D.)

September 2015

Thesis Committee:

Guðrún Arnbjörg Sævarsdóttir, Supervisor
Associate Professor, Reykjavik University

Geir Martin Haarberg, Co-Supervisor
Norwegian University of Science and Technology

Andrei Manolescu
Professor, Reykjavík University

Þröstur Guðmundsson
HRV Engineering

Arne Petter Ratvik, Examiner
SINTEF, Norway

The undersigned

The undersigned hereby grants permission to the Reykjavík University Library to reproduce single copies of this Dissertation entitled **Impurities and Current Efficiency in Aluminum Electrolysis** and to lend or sell such copies for private, scholarly or scientific research purposes only.

The author reserves all other publication and other rights in association with the copyright in the Dissertation, and except as herein before provided, neither the Dissertation nor any substantial portion thereof may be printed or otherwise reproduced in any material form whatsoever without the author's prior written permission.

_____

Date

_____

Rauan Meirbekova
Doctor of Philosophy

To my parents, Bolatbek Meirbekov and Tyulpan Ordabayeva.

Preface

This thesis is submitted to the Norwegian University of Science and Technology and Reykjavik University for partial fulfillment of the requirements for the degree of philosophiae doctor.

This doctoral work has been performed at the Department of Material Science and Engineering, NTNU, Norway and Department of Science and Engineering Reykjavik University, Iceland, with Guðrún A. Sævarsdóttir as a main supervisor and with a co-supervisor Geir Martin Haarberg.

This is an experimental project run as a collaboration between Alcoa Fjarðaál, HRV engineering, Reykjavik University and the Norwegian University of Science and Technology.

Impurities and Current Efficiency in Aluminum Electrolysis

Rauan Meirbekova
September 2015

Abstract

Current efficiency loss in aluminum electrolysis happens due to a variety of factors. One such factor is the presence of impurities. Concerns about impurities have been voiced since the quality of raw materials has declined and dry-scrubbers were installed. The most talked about impurity with detrimental effects on aluminum electrolysis is phosphorus, which can reduce current efficiency by about 1% per each 100 ppm of added phosphorus. The growing trend towards high amperage in aluminum reduction cells may require higher current densities. Therefore, it is of interest to industry to know if the phosphorus effect persists at high current densities.

The main purpose of the thesis was to study the impact of phosphorus under high current density conditions (1.5 A/cm^2) by adding $AlPO_4$ into the electrolyte. Low current density (0.8 A/cm^2) experiments were performed as a control. This study also included experiments at low concentrations of phosphorus (0-220 ppm), which are of particular interest for the industry. The effect of current density on current efficiency up to high current densities was also investigated prior to the experiments with impurities. Additionally, a data analysis campaign was run on operational data from Alcoa Fjarðaál. Daily measurements and operational data (from January 2011 to December 2013 at Alcoa Fjarðaál) were collected and analyzed to improve the understanding of effects of various process parameters (bath height, temperature, superheat, and age) on the concentration of phosphorus in the metal.

A second objective of the thesis was to investigate the effect of sulfur in the bath on current efficiency. This was achieved by adding Na_2SO_4 directly into the electrolyte. Sodium sulfate was found to be very reactive under electrolyzing conditions and required frequent additions.

The results of the current efficiency experiments for phosphorus support previous findings that phosphorus contributes to a decrease in current efficiency by 0.67% at 0.8 A/cm^2. Current efficiency measurements at a high current density of 1.5 A/cm^2 showed a clear negative effect of phosphorus and demonstrated a slightly higher decrease in current efficiency (1.1% per 100 ppm of phosphorus). Regression analysis of data obtained for lower phosphorus concentrations (0-230 ppm) revealed a pronounced current efficiency reduction of 0.92% per 100 ppm of phosphorus at 0.8 A/cm^2 and 2.41% at 1.5 A/cm^2. The detrimental effect of sulfur on current efficiency was confirmed and revealed a 1.1% decrease in current efficiency per 100 ppm of sulfur in the electrolyte.

Experiments with current densities of up to 2 A/cm^2 showed that, although current efficiency increases with increasing current density of up to 1.5 A/cm^2, at higher current densities, the trend reverses and current efficiency is reduced instead. These findings are valid for the specific cell design under investigation, but similar mechanisms may apply in other settings.

Industrial data analysis revealed strong correlations between high phosphorus in the metal and lower superheat, higher bath height, and increased cell age.

Óhreinindi og Straumnýtni í Rafgreiningu Súráls

Rauan Meirbekova

September 2015

Útdráttur

Það er margt sem getur valdið skerðingu á straumnýtni við rafgreiningu súráls. Eitt af því sem haft getur áhrif eru óhreinindi í raflausninni. Uppsöfnun óhreininda í hlöðnu súráli frá þurrhreinsivirki og almennt breytt aðgengi að hreinum hágæða hráefnum fyrir áliðnað hafa bein athyglinni að áhrifum snefilefna á rekstrarþætti. Best þekkta dæmið um snefilefni sem skaðar straumnýtni er fosfór, sem getur skert straumnýtnina um 1% fyrir hver 100 ppm af fosfór í raflausn. Flest álver vinna að því að auka straum um kerskála sína sem þýðir hærri straumþéttleika í rafgreiningarkerjunum. Því er áhugavert fyrir iðnaðinn að vita hvort áhrif forsfórs og annarra óhreininda séu háð straumþéttleika.

Megin markmið þessa verkefnis var að skoða hver áhrif fosfórs væru við háan straumþéttleika (1.5 A/cm^2). Fosfór var bætt út í raflausnina á forminu $AlPO_4$. Samskonar tilraunir voru gerðar við lægri straumþéttleika (0.8 A/cm^2) til samanburðar. Straumnýtnin var mæld fyrir breitt styrkleikabil fosfórs, frá tiltölulega lágum styrkleika eins og algengur er í kerjum í rekstri (0-220 ppm) upp í 1000 ppm. Þessu til viðbótar voru rekstrargögn frá Alcoa Fjarðaál greind tölfræðilega með tilliti til þessara þátta. Gögnum frá janúar 2011 til desember 2013 var safnað og þau greind til að fá upplýsingar um áhrif ýmissa rekstrarþátta (baðhæð, hitastig, yfirhiti, aldur o.s.frv) á styrkleika fosfórs í málminum.

Annað markmið verkefnisins var að skoða áhrif brennisteins í raflausninni á straumnýtninga. Þetta var gert með því að bæta Na_2SO_4 beint í raflausnina. Natríum súlfíð reyndist vera mjög hvarfgjarnt við skilyrði rafgreiningar og þurfti að bæta því reglulega út í raflausnina til að viðhalda því brennisteinsinnihaldi sem miðað var við hverju sinni. Niðurstöður straumnýtnimælinganna styðja fyrri niðurstöður um að fosfór í raflausn skerði straumnýtni og nemur skerðingin að jafnaði 0.67% at 0.8 A/cm^2. Straumnýtnimælingar við hærri straumþéttleika, 1.5 A/cm^2, gáfu þær niðurstöður að áhrif fosfórs væru enn meiri við þær aðstæður með lækkun í straumnýni sem nemur 1.1% fyrir 100 ppm í aukningu fósfórinnihalds. Ef áhrifin á straumnýtni eru skoðuð sérstaklega fyrir tiltölulega lágan styrk fosfórs (0-230 ppm) sást að aukning í fosfórinnihaldi hefur hlutfallslega meiri áhrif eða sem nemur 0.92% fyrir 100 ppm aukningu fosfórs við 0.8 A/cm^2 og 2.41% við 1.5 A/cm^2, þetta bendir til að þeir ferlar sem valda lækkun straumnýni mæti mettun við hærri styrkleika. Sýnt var fram á að brennisteinn í raflausninni veldur skerðingu á straumnýtni sem nemur 1.1% fyrir 100 ppm aukningu í raflausn.

Jafnframt var straumnýtni án viðbættra snefilefna mæld fyrir straumþéttleika allt að 2 A/cm^2. Niðurstaða þeirra mælinga er að straumnýtnin eykst við aukinn straumþéttleika en þó minna eftir því sem þéttleikinn eykst þar til straumþéttnin nær hámarki við 1.5 A/cm^2, en straumnýtnin minnkar ef straumþéttni er hækkuð umfram

það. Þessar niðurstöður gilda fyrir tilraunakerið sem notað var við þessar tilraunir og sýna hvernig flæðisskilyrði i þeirri hönnun breyta aðstæðum til massaflutnings um jaðarlög við hærri straumþéttni. Niðurstöðurnar má því ekki yfirfæra beint á ker í iðnaði en þó gætu sambærilegir ferlar átt sér stað á iðnaðarskala.

Greining rekstrargagna frá Alcoa Fjarðaal sýndu fram á sterka fylgni milli fosfórs í raflausn og lágs yfirhita og hárrar baðhæðar. Einnig fannst fylgni við aldur rafgreiningarkerja.

Acknowledgements

Financial contribution and technical support is very much appreciated from Alcoa Fjarðaál and HRV Engineering. I am grateful for additional funding for sulfur experiments from NTNU and SINTEF.

I wish to express sincere thanks to my supervisor Dr. Guðrún Sævarsdóttir for her guidance and supervision with thesis work. Thank you for giving me this opportunity and I deeply appreciate your help on this work.

For his support and advice, I would like to express my sincere gratitude to my co-supervisor, Professor Geir Martin Haarberg. Thank you for introducing and opening doors to molten salt electrochemistry field, which is truly fascinating.

My deepest and endless thanks goes to the great emeritus Professor Jomar Thonstad for his time, advice, questions, answers, suggestions, ideas and interest in this work.

I would like to thank Professor Andrei Manolescu from Reykjavik University for his practical guidance and countless hours of helpfulness. I would like to thank Reykjavik University library, particularly Unnur Valgeirsdóttir with providing all necessary literature.

I would like to thank Alcoa Fjarðáal staff, Steinunn Ingimarsdóttir, Atli V. Hjartarson, Julius Brynjarsson, Kristinn M. Ingimarsson, G. María Jóhannsdóttir, and Valgerður Yngvadóttir for their help and assistance with experiments. I am deeply grateful for warm welcome and becoming my friends. Special thanks to Dr. Donald Ziegler and Julie Young (Alcoa Technical Center) for their guidance on performing industrial experiments.

I would like to thank SINTEF for permission to conduct experiments in their laboratory and also for all the assistance along with experiments. Thanks a lot for Arne Petter Ratvik, Thor Aarhaug, Ole Kjos, Asbjørn Solheim, Karen Osen, Ove Darell, Henrik Gudbrandsen, Egil Skybakmoen, Ana M. Martinez, and Sverre Rolseth.

I would like to express my sincere gratitude to Dr Lorentz Petter Lossius and Karin Bolstad from Hydro Aluminium for sample analysis using XRD.

For technical assistance and material supply for the laboratory experiments, I would like to thank Aksel Alstad, Kjel Røkke, and Solveig Jonassen. I would like to thank also Elin Synnøve Isaksen Kaasen and Anne Sæther for all help with documents.

I am indebted to master students Petre Manolescu and Anna Torfte who have assisted me with laboratory experiments.

I would like to thank my University colleagues who have contributed to this thesis directly and indirectly: Mark Kennedy, Wenting Xu, Samuel Perkin, Laurens van der Werff, Ahmet Tezel, Svetlana Kalyavina, Rebecca Thorne, Camilla Sommerseth,

Henrik Åsheim, Marjan Ilkov, Lahcen Bouhlali, Vijay Chauhan, Yonatan A. Tesfahunegn, Einar J. Erlingsson, Maria S. Gudjonsdottir, Joseph T. Foley, David James Thue and Stephan Schiffel.

Finally, I would like to thank my husband, Bjarki Gunnarsson, my parents, Tyulpan Ordabayeva and Bolatbek Meirbekov, my brother, Serik Meirbekov and sister, Aruzhan Kaliyeva and my sons, Joel Nur Bjarkason and Nói Páll Bjarkason, for everything they have sacrificed for me. I would like also say a giant thank you to my parents-in-law, Gunnar Böðvarsson and Sigrún Sigfúsdóttir, for all the help and support.

Contents

Preface ..... **ix**

Abstract ..... **xi**

Acknowledgements ..... **xv**

Contents ..... **xvii**

List of symbols and abbreviations ..... **xix**

Symbol Meaning xix
Abbreviation Meaning xx

1 INTRODUCTION **1**

2 BACKGROUND **5**

2.1 Hall- Héroult Process and Current Efficiency *5*
2.1 Impurities *8*
2.1.1 Phosphorus 8
2.1.2 Sulfur 14

3 EXPERIMENTAL **25**

3.1 Methodology and Experimental Set-Up (Supplements 1, 2, 3 & 5) *25*
3.1.1 Choice of Cell Design 25
3.1.2 Materials 26
3.1.3 Procedure 28
3.1.4 Choice of Method for Determination of Current Efficiency 30
3.2 Methodology and Experimental Set-Up for Industry-Scale Experiments (Supplement 4) *31*
3.2.1 Data Analysis Methods 31
3.2.2 Experimental Sampling Device 32
3.2.3 Procedure 35
3.3 Methodology and Experimental Set-Up for the Sulfur Experiment (Supplement 6) *35*
3.3.1 Experimental Set-Up and Procedure 35
3.3.2 Gas Analysis Method 36
3.4 Analytical Methods *37*

4 RESULTS AND DISCUSSIONS **39**

4.1 Laboratory Studies *39*
4.1.1 Effect of Current Density on Current Efficiency (Supplements 1-3) 39
4.1.2. Effect of Phosphorus on Current Efficiency 41

4.1.2.1 Phosphorus Concentration during the Experiments *(Supplement 3)* . 41
4.1.2.2 Effect of Phosphorus on Current Efficiency *(Supplement 3)* 43
4.1.3 Effect of Sulfur on Current Efficiency 45
4.1.3.1 Sulfur Concentration during the Experiments *(Supplement 5)*..... 45
4.1.3.2 Effect of Sulfur on Current Efficiency *(Supplement 5)* 48
4.1.3 Behavior of Sodium Sulfate in Cryolite-Alumina Melts (*Supplement 6*). 51
4.2. Industrial Studies *57*
4.2.1. Plant Data Analysis (*Supplement 4*) 57
4.2.2 Behavior of Impurities during Current Interruption (*Supplement 4*)..... 59
4.2.3. Sodium Sulfate Addition Tests (*Supplement 6*)..... 61

5 FUTURE WORK AND CONCLUSION 65

5.1 Future Work *65*
5.2. Conclusions *65*

6 REFERENCES..... 69

SUPPLEMENT 1 77

SUPPLEMENT 2 79

SUPPLEMENT 3 81

SUPPLEMENT 4 83

SUPPLEMENT 5 85

SUPPLEMENT 6 87

List of symbols and abbreviations

Symbol	Meaning	Units
$c_{P,bath}$	Phosphorus concentration in the bath	ppm
$c_{P,metal}$	Phosphorus concentration in the metal	ppm
c_s	Concentration of sulfur	ppm
$c_{s(max)}$	Maximum concentration of sulfur	ppm
$c_{s(min)}$	Minimum concentration of sulfur	ppm
$E°$	Standard potential	V
E_d	Decomposition potential	V
F	Faraday's constant	C/mol
$\Delta G°$	Standard Gibbs reaction energy	kJ/mol
$\Delta_{rx}G$	Gibbs energy of reaction	kJ/mol
I	Current	A
i_c	Cathodic current density	A/cm^2
i_{loss}	Loss current density	A/cm^2
ln	Natural logarithm	
m	Mass	g
m_{actual}	Actual mass	g
$m_{ltheory}$	Mass theoretically derived from Faraday's law	g
M	Molar mass	g/mol
N	Sample size	
r_{theory}	Theoretical rate of production	mg/s
r_{actual}	Actual rate of production	mg/s
r_{actual}	Rate of reoxidation reaction	mg/s
t	Time	min
$t_{1/2}$	Half-life	min
T	Temperature	°C or K
z	Valence of the product	
σ	Population standard deviation	
Ø	Diameter	m

Abbreviation	Meaning
ACD	Anode cathode distance
Al	Aluminum
CE	Current efficiency (%)
CR	Cryolite ratio
C	Carbon
DS	Dry scrubber
El	Electrolysis
ISW	Iron spatula white
ICP-AES	Inductively coupled plasma – atomic emission spectrometry
MHD	Magneto hydro dynamics
ppm	Parts per million
ppmv	Parts per million by volume
SEM	Scanning electron microscope
XRF	X-ray fluorescence
XRD	X-ray diffraction

1 INTRODUCTION

A typical aluminum smelter consists of multiple Hall-Héroult cells and has high construction and operational costs. It is therefore important that the production process is managed efficiently and that aluminum is produced with high productivity. In the last few decades, smelters have been focusing on increasing productivity by increasing pot line amperage and current efficiency and by reducing energy consumption.

To increase pot line amperage in industrial cells, higher current densities may be required. The advantage of increasing current density is that higher productivity can be achieved without changing the footprint of the plant. Therefore, one part of our study investigated electrochemical processes at high current densities. It provides results that are of interest today.

Current efficiency is an important cell parameter that describes what fraction of the electric current actually results in aluminum production. Current efficiency in Hall-Héroult cells has improved significantly since the cell's invention and can be as high as 96% today. Additional improvements can be made by managing marginal contributing factors such as impurities [1]. Impurities are introduced into the process mainly from raw materials required for aluminum production. Gradual deterioration of raw material quality in recent years has caused increased concern regarding the effects of impurities on the production process. Additionally, installation of dry scrubbers resulted in increased recycling of flue gas impurities back into the cell. Many of these impurities end up in the produced metal. This resulted in new challenges not only with respect to metal quality but also cell performance. One of the well-known detrimental impurities is phosphorous. It has been reported that a 1% decrease in current efficiency can be expected for each 100 ppm of phosphorus in the electrolyte [1-4].

The primary objective of the thesis is to contribute to the understanding of the effects of detrimental impurities in aluminum electrolysis, particularly with respect to current efficiency. The first part of the thesis focuses on studying the effect of phosphorus on current efficiency. Next, we investigated the effect of phosphorus at higher current densities and at concentrations present in industry (0-240 ppm). Industrial data pertaining to phosphorus concentration were utilized to understand pot-to-pot variability.

The topic for the second part of the thesis is sulfur. Sulfur is mainly introduced to the cells by anodes. Over the last decade, availability of low sulfur anodes has been reduced due to changes in crude oil quality [5]. This has raised marked interest in the question of whether any negative effects of increased anode sulfur levels exist. Most of the available literature only considered the effects of sulfur on carbon consumption [6-9] and viewed sulfur contamination positively due to the ability of sulfur to poison the catalytic effect of other impurities. Very little literature on the effect of sulfur on

current efficiency is available. An earlier study concluded that there was no effect on current efficiency [10], while a recent study found that increasing sulfur content contributes significantly to current efficiency reduction [11].

The objective of the thesis was to further the understanding of the behavior of phosphorus and sulfur in Hall-Héroult cells and the effect these impurities have on process parameters. This goal was achieved through the following activities:

1. studying the effect of current density on current efficiency in a laboratory cell,
2. performing a study on the effect of phosphorus on current efficiency at low (0.8 A/cm^2) and high (1.5 A/cm^2) current densities,
3. correlating cell process parameters with phosphorus concentration in produced aluminum by analyzing registered daily measurements from the Alcoa Fjarðaál smelter,
4. determining whether there is any effect of sulfur on current efficiency by performing laboratory experiments with sodium sulfate added as a sulfur source, and
5. investigating sodium sulfate behavior in cryolite-alumina melts under different conditions and measuring the produced gases.

This thesis includes the following publications, appended as supplements:

Supplement 1: *R. Meirbekova, G.M. Haarberg and, G. Saevarsdottir, Effect of Phosphorus Impurities on the Current Efficiency for Aluminium Deposition from Cryolite-Alumina Melts in a Laboratory Cell, in Molten Salts Chemistry and Technology, John Wiley & Sons, pp. 71-75.*

In this paper, previous research performed by Solli [2] and Thisted [1] at 0.8 A/cm^2 were used as a reference. New experiments were performed at a higher current density of 1.5 A/cm^2. Other parameters were selected to match Solli [2] and Thisted [1]. Additionally, the effect of current density on current efficiency was investigated. The results of the study show that phosphorus in the bath reduced current efficiency at a high current density (1.5 A/cm^2) and resulted in a similar reduction in current efficiency (by 0.81% per 100 ppm of added phosphorus). Current efficiency increased slightly when current density was changed from 0.8 to 1.5 A/cm^2.

Supplement 2: *R. Meirbekova, G. Saevarsdottir, G.M. Haarberg and J.P. Armoo, "Effect of Current Density and Phosphorus Impurities on the Current Efficiency for Aluminum Deposition in Cryolite-Alumina Melts in a Laboratory Cell", Light Metals 2013, pp. 917-920.*

This paper expands on the work in *Supplement 1*. The method of phosphorus addition into the bath raised a few concerns because some powder was expelled by nitrogen gas during addition. To address this, a decision was made to confirm phosphorus concentration after termination of each experiment. The solidified bath was removed from the crucible and analyzed for phosphorus concentration by ICP (Inductive Coupled Plasma). The measured phosphorous values deviated from the

predicted values based on the amount of phosphorus introduced. When current efficiency was plotted as a function of the measured concentrations, the current efficiency decrease was greater than previously reported. Current efficiency now decreased by 3.8% per 100 ppm of phosphorus in the bath. The current efficiency calculated by using ICP measurements should be more accurate than the calculations using theoretical amounts of phosphorus added. However, calculations performed at the termination of experiments are likely to overestimate the slope due to the fact that the average phosphorus concentration is probably higher than the concentration at termination. This highlights the importance of verification of phosphorus concentration during the course of the experiments.

Supplement 3: *R. Meirbekova, J. Thonstad, G.M. Haarberg and G. Saevarsdottir, "Effect of Current Density and Phosphorus Species on Current Efficiency in Aluminium Electrolysis at High Current Densities", Light Metals 2014, pp. 759-764.*

The limitations of the previous study were addressed in this paper. Phosphorus concentration was monitored by continuous sampling of the bath. It was found that phosphorus concentration initially dropped very little and afterwards remained relatively constant. Solidified bath samples taken after the termination of the experiments were compared with samples removed during the course of the experiments. Results confirmed that concentrations derived from the solidified bath were not representative due to segregation during solidification. The detrimental effect of phosphorus on current efficiency was found to be significant at concentrations below 220 ppm. The effect was even more pronounced at higher current density (1.5 A/cm^2) compared to lower current density (0.8 A/cm^2). The observed reduction was 2.41% ± 0.45% per 100 ppm of phosphorus at 1.5 A/cm^2, whereas at 0.8 A/cm^2 it was 0.92% ± 0.16% per 100 ppm of phosphorus for the same range of concentrations. The reduction at higher concentrations was in agreement with literature (0.68% at 0.8 A/cm^2 and 1.05% at 1.5 A/cm^2).

Supplement 4: *R. Meirbekova, G.M. Haarberg, J. Thonstad, Donald P. Ziegler, J. Brynjarsson and G. Saevarsdottir, "Effect of Operational Parameters on the Behaviour of Phosphorus and Sulfur on Aluminium Reduction", Light Metals 2015, pp. 559-564.*

This paper reports the results of data analysis performed on registered data from three years of daily measurements at the Alcoa Fjarðaál smelter. A number of process parameters were analyzed with respect to phosphorus concentration in the metal. Additionally, experimental samples taken during power outages were collected and analyzed for sulfur and phosphorus concentrations in the bath. This study contributes to an understanding of pot-to-pot variability of phosphorus and its behavior at different conditions. Phosphorus concentration in the metal was found to correlate with the height of the bath, superheat, and age of the cell. Elemental analysis showed an increase in phosphorus and sulfur concentrations during power outages.

Supplement 5: *R. Meirbekova, G.M. Haarberg, J. Thonstad, and G. Saevarsdottir, "Influence of Sulfur Species on Current Efficiency in the Aluminum Smelting Process", submitted to Metallurgical and Material Transaction B.*

This paper answers the frequently asked questions on whether sulfur has an effect on current efficiency in a laboratory setting. The study was performed in a laboratory cell by direct additions of sodium sulfate into the bath. Sodium sulfate was found to be very reactive in aluminum reduction cells. As a result, it was added at regular time intervals to maintain a constant concentration. Current efficiency was reduced by approximately 1% per each 100 ppm increase in sulfur concentration.

Supplement 6: *R. Meirbekova, G.M. Haarberg, T. A. Aahaug, J. Thonstad, and G. Saevarsdottir, "Behavior of Sodium Sulfate in Cryolite-Alumina Melts and the Formation of Sulfurous Gases", submitted to ECS Transactions.*

This paper contributes to the understanding of sodium sulfate behavior in cryolite-alumina melts. Stability of sodium sulfate in cryolite melts is studied and found to depend on the presence of carbon and aluminum and occurrence of electrolysis. Electrolysis was the strongest factor. Gas analysis was performed to understand the gaseous byproducts formed. Results indicated that CS_2 can be formed when there is a source of sulfur and carbon in the electrolyte. COS was also formed following CO_2 production. The last finding was that addition of sodium sulfate to industrial cells increased cell resistance.

2 BACKGROUND

2.1 Hall- Héroult Process and Current Efficiency

In 1886, two scientists, Paul Héroult in France and Charles Hall in the USA, independently invented the electrolytic process for aluminum production. Héroult and Hall separately applied for patent registration for producing liquid aluminum by electrolysis of a molten solution of alumina (Al_2O_3) in cryolite (Na_3AlF_6) [12].

The two scientists had different approaches to discovering the aluminum production process. Héroult came up with the idea by looking for suitable raw material (alumina) for the cryolite. Hall, on the other hand, decided to use alumina from the start and was searching for an appropriate solvent. He tried different salts until he found cryolite.

The production process is named "The Hall-Héroult Process" after both inventors. In the process, liquid aluminum is produced by electrolytic reduction of alumina dissolved in cryolite. Despite many studies and attempts to replace the process with something new, the Hall-Héroult process continues to be the only method by which aluminum is produced industrially today.

Besides cryolite and alumina, the electrolytic bath may contain other additives: 6-13 wt% aluminum fluoride (AlF_3), 4-6 wt% calcium fluoride (CaF_2), 2-4 wt% lithium fluoride (LiF), and 2-4 wt% magnesium fluoride (MgF_2) [13]. Some of the additives enter the bath with raw materials while others are added intentionally. These additives modify bath properties by lowering density and vapor pressure or by giving higher interfacial tension and electrical conductivity. Typical bath temperature ranges from 940 to 970 °C depending upon bath composition [13].

Two anode designs exist: prebaked and Söderberg. Prebaked anodes are made of a mixture of petroleum coke aggregate and coal tar pitch binder shaped into blocks. These blocks are baked at 1100-1200 °C prior to use as cell anodes [14]. Prebaked anodes are consumable, and they have to be replaced approximately on a monthly basis. Remains of used anodes are called butts. These have to be removed from the cells and recycled in butts-cleaning stations where they are cleaned, crushed, and reused to make new anodes. Söderberg anodes are continuously self-baked in situ and do not have to be replaced. They are composed of calcined petroleum coke and coal-tar or petroleum pitch [14]. Green anode briquettes are added to the tops of the anodes and are subsequently melted and baked by the heat from the cell as the materials are moving downwards to the electrolyte interface and being consumed. The disadvantage of this process is that it is hard to efficiently collect off-gases because of the cell design. The size of cells utilizing Söderberg anodes is also limited.

The use of Söderberg anodes for aluminum production is fading away, and this thesis focused only on prebaked cells.

Inside the cell, electric current passes vertically down from carbon anodes to a carbon cathode, melting the alumina and the cryolite. The overall primary cell reaction for aluminum production is [13]:

$$1/2\ Al_2O_3 + 3/4C = Al + 3/4CO_2 \tag{2.1}$$

As result of thermal, electrical, magneto-hydrodynamic, and electrochemical processes, the dissolved alumina oxide ions react with the carbon anode producing CO_2 while aluminum is produced at the cathode [15]. The anode is consumed over time, and aluminum accumulates in the liquid metal pool at the bottom of the bath. The resulting layer of liquid aluminum metal becomes the effective cathode. The entire cathode consists of the carbon cathode blocks with current collector bars. Underneath the cathode, there are refractories and insulation placed inside a supporting steel shell [16].

Aluminum production requires consumption of electrical energy. The concept of current efficiency describes how efficiently electrical current is used to produce aluminum in the cell. Current efficiency is governed by Faraday's laws and states that the quantity of product, m (grams), formed at each electrode is proportional to electrical charge (measured in Coulombs) passing through the cell and to the equivalent molar mass of the product [13].

Faraday's law is expressed with the following equation [13]:

$$m = \frac{M}{zF} It \tag{2.2}$$

F= 96485 C mol^{-1} is Faraday's constant, M is molar mass, z is valence of the product, I is current, and t is time. Current efficiency is the ratio of the actual mass of metal produced and the mass theoretically derived from Faraday's law [13]:

$$CE\% = \frac{m_{actual}}{m_{theory}} \tag{2.3}$$

An alternative to expressing current efficiency is to use cathodic current density (i_c) consumed for the formation of the product divided by total cathodic current density, which is the sum of the cathodic current density and the current density loss (i_{loss}) due to parasitic reactions [14]:

$$CE\% = \frac{i_c}{i_c + i_{loss}} \tag{2.4}$$

The primary cause of current efficiency loss is the so-called back reaction between dissolved metal and carbon dioxide. It is defined by following reaction [13, 14]:

$$Al + 3/2CO_2 = 1/2Al_2O_3 + 3/2CO \quad (2.5)$$

According to [17], modern description of back reaction involves the following reactions that contribute to the current efficiency loss:

Cathode reaction:

$$AlF_3 + 3Na^+ + 3e^- = Al + 3NaF \quad (2.6)$$

Anode reaction:

$$1/2Al_2O_3 + 3/4C + 3NaF = AlF_3 + 3/4CO_2 + 3Na^+ + 3e^- \quad (2.7)$$

Side reaction:

$$3Na^+ + 3e^- = 3Na_{diss} \quad (2.8)$$

Back reaction:

$$3Na_{diss} + 3/2CO_2 + AlF_3 = 3NaF + 1/2Al_2O_3 + 3/2CO \quad (2.9)$$

Total back reaction:

$$3Na^+ + 3e^- + 3/2CO_2 + AlF_3 = 3NaF + 1/2Al_2O_3 + 3/2CO \quad (2.10)$$

AlF_3^- in the above equations includes aluminum containing complexes (AlF_4^-, AlF_6^{3-}).

The rate-determining step for the back reaction is the diffusion of dissolved metal through the boundary layer. The back reaction takes place outside of the cathodic boundary layer [14].

The rate of the back reaction can be increased by reduced diffusion layer thickness and increased mass transfer. Cell stability therefore plays an important role [13]. Improvements in magnetic compensation designs have significantly contributed to increases in current efficiency [18, 19].

The rate of the back reaction also increases with the concentration of dissolved metal at the interface. As such, the back reaction is strongly connected to metal solubility [14]. Dissolved sodium is regarded as more important due to higher concentrations of dissolved Na than dissolved Al in industrial type electrolytes. This is a result of sodium's electronic properties and the high mobility of its associated electrons [17]. More NaF in the bath will increase the solubility of Na. On the other hand, an increase in the concentration of AlF_3 decreases liquidus temperature. Consequently, metal solubility is reduced and current efficiency increases. Other additives such as CaF_2, LiF, and MgF_2 show similar effect. The biggest challenge to improving current efficiency by lowering temperature is a concurrent reduction in alumina solubility.

Other processes that may contribute to current efficiency loss are formation and subsequent oxidation of aluminum carbide [20], oxidation of disperse aluminum droplets [21, 22], electronic conductivity [23-25], metal shorting [26], and the presence of multivalent impurities such as phosphorus [27].

2.1 Impurities

The main interest of the thesis is the effect of impurities on current efficiency. This is of heightened importance since dry scrubber implementation and deterioration in raw material quality. This thesis focuses particularly on the behavior of phosphorus and sulfur in aluminum electrolysis cells. The impurities enter the cell by continuous feed of raw materials, alumina, and carbon anodes. Small amounts of AlF_3 have to be added to compensate for evaporation losses and to maintain constant bath composition. Impurities can also be introduced by handling tools or corrosion of structural components of the cell. Depending on their nature, impurities can influence the process in different ways, causing excess carbon consumption, deterioration of materials, changes in electrolyte composition, or reduce current efficiency and affect metal quality [27].

2.1.1 Phosphorus

Phosphorus originates mostly from alumina due to the frequent feeding rates although it is found at higher concentrations in other raw materials. **Table 2.1** shows typical concentrations of phosphorus in raw materials.

Table 2.1: Contents of phosphorus expressed as P_2O_5 in different raw materials, values in ppm.

Al_2O_3	Secondary Al_2O_3	AlF_3	Na_3AlF_6	Anode
4-11 [14]	65 [14]	160-210 [28]	150-200 [14]	7-23 [29]

Phosphorus comes from alumina in the form of P_2O_5 or $AlPO_4$ [30]. Existence of other compounds in alumina such as $Al(PO_3)_3$, Na_3PO_4, and Fe_2P were also suggested [31, 32]. Phosphorus can have many oxidation states from -3 up to +5. In the electrolyte, it is most likely present in the oxidation state of +5 [30].

Stability of phosphorus containing compounds in the cryolite melt was of interest to many researchers. As a result, many phase diagrams with phosphorus compounds and cryolite exist. Del Campo [33] and Bratland et al. [34] reported studies on $Na_4P_2O_7$-Na_3AlF_6. Chrenkova et al. [35] made measurements on Na_3PO_4 - Na_3AlF_6 and $AlPO_4$- Na_3AlF_6 systems. Thisted et al. [36] and Kucharík et al. [37], determined the stability and solubility of $AlPO_4$ in Na_3AlF_6.

Reactions of phosphorus compounds (P_2O_5 or $AlPO_4$) in the electrolyte and dry scrubber compiled from literature [1] are listed in **Table 2.2** and **Table 2.3,** respectively. Only reactions with negative Gibbs energies are shown. $Al(PO_3)_3$ was not found in the database of HSC 7.1 software and is therefore not included in the table.

Table 2.2: Reactions of phosphorus compounds in electrolyte at 980 °C [1]. Gibbs free energies for the reactions were calculated by using HSC 7.1 software.

Na_2AlF_6 /AlF_3	$\Delta_rG°$ (kJ/mol)	
$P_2O_{5(g)} + 2AlF_{3(l)} = Al_2O_3 + 2POF_{3(g)}$	-245	(2.11)
Al_2O_3		
$P_2O_{5(g)} + Al_2O_3 = 2\ AlPO_4$	-389	(2.12)
C		
$P_2O_{5(g)} + C = P_2O_{3(g)} + CO_2$	-139	(2.13)
$P_2O_{5(g)} + 5/2C = P_{2(g)} + 5/2CO_2$	-167	(2.14)
Al		
$P_2O_{5(g)} + 16/3Al_{(l)} = 2AlP + 5/3\ Al_2O_3$	-1445	(2.15)
$P_2O_{5(g)} + 10/3Al_{(l)} = 5/3\ Al_2O_3 + 2P_{(g)}$	-960	(2.16)
$P_2O_{5(g)} + 10/3Al_{(l)} = 5/3\ Al_2O_3 + 2P_{(s)}$	-1295	(2.17)
$AlPO_4 + 5/3\ Al_{(l)} = 4/3\ Al_2O_3 + P_{(g)}$	-285	(2.18)
$AlPO_4 + 5/3\ Al_{(l)} = 4/3\ Al_2O_3 + P_{(s)}$	-452	(2.19)
$AlPO_4 + 8/3\ Al_{(l)} = AlP + 4/3\ Al_2O_3$	-527	(2.20)
$AlPO_4 + 5/3Al_{(l)} = ½\ P_{2(g)} + 4/3\ Al_2O_3$	-459	(2.21)

The above reactions (2.16-2.22) indicate that phosphorus compounds can react with aluminum and cause metal loss. Chaudhuri [38] performed experiments where aluminum loss was studied by adding impurities into the cryolite melt without electrolysis. He reported increased loss of aluminum in the presence of phosphorus.

Table 2.3: Reactions in the dry scrubber unit at 100 °C [1]. Gibbs free energies for the reactions were calculated using HSC 7.1 software.

	$\Delta_r G°$ (kJ)	
$POF_{3(g)} + Al_2O_3 = AlPO_4 + AlF_3$	-249	(2.22)
$P_2O_{5(g)} + 2Al_2O_3 = 2AlPO_4$	-579	(2.23)
$PF_{5(g)} + 4/3\ Al_2O_3 = AlPO_4 + 5/3\ AlF_3$	-361	(2.24)

According to thermodynamic calculations by Thisted [1], phosphorus oxide compounds are considered to be more noble than alumina with standard decomposition potentials $E^o(P_2O_5)$ = +0.1 V and $E^o(Al_2O_3)$ = -1.16V, respectively, at 1020 °C. Danek et al. [31] presented the following reactions, which can possibly explain the mechanism by which phosphorus can cause loss in current efficiency:

$$AlPO_4 + 2C = Al + P_{(g,\ s)} + 2CO_2 \quad (2.25)$$

$$2Al(PO_3)_3 + 9C = 2Al + 6P_{(g,\ s)} + 9CO_2 \quad (2.26)$$

The decomposition potentials for Reactions 2.26 and 2.27 are -0.832 V and -0.221 V at 1200 K, respectively. Accordingly, phosphorus should be expected in the metal phase, but this is not the case. We observed accumulation of phosphorus compounds in the bath and only a limited amount (approximately 10% of all the phosphorus in the bath) was deposited with the aluminum [30]. The low solubility of phosphorus can probably explain the low concentrations found in the metal. The solubility of phosphorus in aluminum at 660 °C is 0.01 wt% [39]. Nevertheless, Grjotheim et al. [12] stated that even low concentrations of phosphorus result in increased brittleness and reduced corrosion resistance.

Reduced current efficiency due to the presence of phosphorus cannot be attributed only to chemical and electrochemical deposition reactions discussed above. Red-ox reactions, where phosphorus is reduced at the cathode and oxidized at the anode, should likewise be considered [14].

Interest in phosphorus has grown considerably since the introduction of dry-scrubbers, which recycle phosphorus back into the cell. Frankenfeldt and Mannweiler [40] correlated collection efficiency of pot hoods and the purity of produced metal. They reported that phosphorus appeared to be present as a volatile compound and therefore high collection efficiencies of the hood result in a high distribution

coefficient of 8.2 between gas and metal/bath. Later, Albers and Wrigge [41] reported a significant increase in phosphorus of up to 300 ppm P_2O_5 in the bath. They found that this caused a decrease in current efficiency of 1% per 100 ppm. Analysis of their electrolyte samples showed that the concentration of phosphorus is proportional to the amount of carbon particles in the electrolyte. Oblakowski and Pietrzyk [42] also reported a linear relationship between phosphorus and carbon concentration. Albers and Wrigge [41] concluded that phosphorus content in the electrolyte depends on openings in the closed looped system (eg. collection efficiency, scrubbing efficiency, dust losses at recycling streams, and produced aluminum). They presented a relationship between concentration of phosphorus in the bath and metal for closed loop systems:

$$c_{P,bath} = \frac{130}{21} c_{P,metal} + 10\ ppm\ P \tag{2.27}$$

where $c_{P,bath}$ is phosphorus concentration in the bath (ppm), $c_{P,metal}$ is phosphorus concentration in the metal (ppm), and P is phosphorus. Böhm et al. [43] confirmed that phosphorus is volatile and 72% of phosphorus compounds escape in the gas phase. The more volatile the phosphorus, the more it will be recycled back with secondary alumina after dry scrubbing. Augood [44] reported that 90% of P can be expected to leave as gas (gas/feed constant was equal to 0.91). The dry scrubber recycle system thus has a potential to move a lot of phosphorus into the bath and consequently into the metal [44].

Considerable research has been done to remove phosphorus from secondary alumina by various techniques such as electrostatic precipitation (removal efficiency of 90%) [43], selective impact milling (70%) [45], magnetic separation [32], ultrasonic vibration (75-85%) [46, 47], flotation (80%) [46], chemical treatment (30-50%) [46], and installation of primary cyclones (48%) [48]. Most of these techniques were based on removal of impurities by grain size fraction, as the fine fraction alumina contains about 50% of impurities [32]. However, smelters do not find installation of such units economically feasible.

Øye [28] carried out mass balances for impurities in a cell with prebaked anodes and a dry scrubber. According to the output scheme, 65% of phosphorus goes into the anode cover and cell off-gas, 15% leaves via anode butts, 10% ends up in the metal, and the remainder accumulates in the bath. The distribution factor of phosphorus between aluminum and alumina was found to be less than 0.1.

Danek et al. [31] has performed mass balance for phosphorus distribution in prebaked cells. According to the results, primary alumina contained phosphorus at a concentration of 3.8 ppm, secondary alumina from the dry scrubber contained 33 ppm of phosphorus, the bath had 39 ppm, and the metal 3.5 ppm.

Another mass balance for a prebaked cell with a dry scrubber was done by Haugland et al [30], who concluded that 80% of phosphorus entering the process via primary alumina will leave the cell through aluminum. They also studied the effect of

various process parameters on the concentration of phosphorus in the bath. A small increase in temperature was found to enhance evaporation of phosphorus in the bath and thus reduce its concentration in the metal. Anode effect and anode change also influenced phosphorus concentration in the metal. Anode effect can increase temperature and convection and consequently facilitate the escape of phosphorus by evaporation. The decrease during anode change was explained by direct escape of phosphorus into the air during periods of exposure of the bath to the atmosphere. The authors also tested retention time of different impurities (Fe, Si) added together with $AlPO_4$ and Na_3PO_4 into industrial pots. Compared to other impurities, phosphorus concentration decayed much slower. The slow decay of phosphorus was explained by formation of gaseous phosphorus at the cathode. Most of which leaves the cathode and oxidized by dissolved CO_2 in the bath. This cycle can be repeated several times and hence phosphorus stays in the electrolyte longer and causes current efficiency reduction.

Frolova et al. [49] investigated the behavior of phosphorus in industrial cells. They reported that phosphorus was not accumulating in the electrolyte (likely no dry scrubbers). Half of the phosphorus escaped with off-gas, and the rest was removed by absorbance to carbon dust. The phosphorus improved wettability of carbon dust in the electrolyte and inhibited combustion. This caused difficulties in removing carbon dust from the electrolyte. Consequently, cell resistance and energy consumption increased and electrolyte temperature rose from 962 to 972 °C.

The reduction in current efficiency cannot be concluded to be exclusively due to the presence of phosphorus as other process parameters (temperature, superheat, bath composition, etc.) may have also had an effect. The most reliable method to determine if there is an effect of phosphorus on current efficiency is to study it in the laboratory where all other parameters can be controlled. Such laboratory studies were performed by Solli et al. [2], Deninger [4], and Thisted [1]. All experiments were performed at 0.8 A/cm^2. Both Solli and Deninger added P_2O_5, but Thisted added $AlPO_4$.

Deninger and Gerlach [4] proposed that below 1200 ppm phosphorus will be reduced to three valent as follows:

$$P^{5+} + 2e^- = P^{3+} \tag{2.28}$$

Reduction to elemental phosphorus occurs at higher concentrations:

$$P^{5+} + 5e^- = P^0 \tag{2.29}$$

Both these products (P^{3+}, P^0) can be reoxidized at the anode. An earlier study of Kerouanton et al. [50] and Charlot et al. [51] also observed a reduction of five-valent phosphorus to three valent through a two electron exchange.

Figure 2.1 shows the results of Solli [2] and Thisted [1] on current efficiency versus the amount of phosphorus added. Solli's study [2] shows that current efficiency is reduced by 0.7% for each 100 ppm phosphorus and Thisted results [11] show a decrease in current efficiency by 0.8% for each 100 ppm of phosphorus.

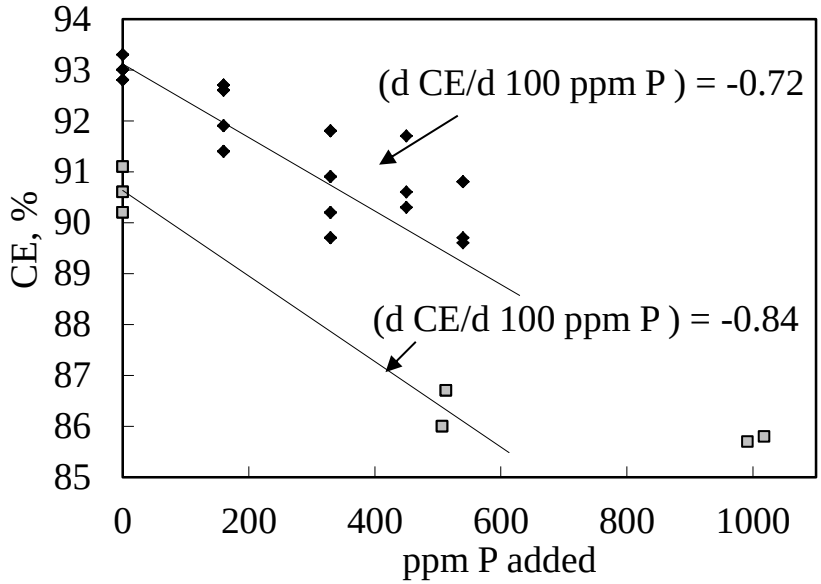

Figure 2.1: Current efficiency versus the amount of phosphorus added; results from Solli [2] are filled diamonds and results from Thisted [1] are grey squares [1].

The reported results [1-4] are in agreement with industrial observations [41] (about a 1% decrease in current efficiency per 100 ppm P). It was concluded that current efficiency loss was a result of cyclic red-ox reactions that consume electricity without producing aluminum.

Keppert [52], motivated by the fact that phosphorus has a detrimental effect on current efficiency, studied the electrochemical behavior of phosphorus in cryolite melts by cyclic voltammetry and chronoamperometry. He reported that phosphorus reduction proceeds in two steps. The first reduction step is reversible and diffusion controlled:

$$PO_4^{3-} + 2e^- = PO_3^{3-} + O^{2-} \quad (2.30)$$

The second reduction step is irreversible and proceeds simultaneously with aluminum reduction via the following equation:

$$PO_3^{3-} + 2e^- = PO_2^{3-} + O^{2-} \quad (2.31)$$

The possibility of formation of elementary phosphorus was also mentioned. Keppert concluded that the first step is the main contributor to the loss in current efficiency.

This thesis further studied the effect of phosphorus on current efficiency at higher current density (1.5 A/cm^2). Industrial experiments and data analysis were done to understand pot-to-pot variability in phosphorus concentration.

2.1.2 Sulfur

Sulfur is introduced to the cell mainly via carbon anodes (80%). The rest comes from alumina (20%) and aluminum fluoride (1%) [12]. Sulfur content in the anode can range from 1 to 4 wt% depending on the type of coke [53]. Anodes are usually prepared by a mix of calcined petroleum coke (or pitch coke) and recycled butts, bound together with coal tar or petroleum pitch [54]. Petroleum coke is the main origin of sulfur in aluminum electrolysis cells [55].

Calcined petroleum coke is made by calcining green petroleum coke at temperatures of ~1200 °C. The green petroleum coke is produced by delayed coking. In delayed coking process crude oil is distilled for petroleum refining, and the remaining residue, a green petroleum coke is sold as the raw material to the aluminum industry for anode production. Sulfur occurs naturally in crude oil in the form of more than 1500 sulfur compounds, predominantly organic (5- and 6-ring structures) [56]. As the supply for quality oil to be refined diminishes, an increase in sulfur concentration in petroleum cokes for the aluminum industry is expected. **Table 2.4** shows a typical impurity profile in petroleum coke [14].

Table 2.4: A typical impurity profile in petroleum coke (ppm) [14]

Impurity	Content	Impurity	Content
Si	50-250	B	1
Fe	50-400	Na	30-120
Ti	2-50	Mg	100
Zn	2-20	Ca	20-100
V	30-350	Mn	4
Cr	1-2	Ga	14
Ni	50-220	Pb	3
Cu	1-3	Al	50-250
S	5000-35000	Ash	1000-2000

Hay et al. [57] studied sulfur speciation in different petroleum cokes using XANES (X-Ray absorption near edge structure) spectroscopy. The synchrotron measurements provided detailed chemical and microstructural information, which helped elucidate the nature of sulfur and its speciation in carbon anodes [58]. According to the results [57], the cokes preserve dominant organic ring structures inherited from crude oil such as five-membered ring thiophenic sulfur

(dibenzothiophene, thianaphene-2-carboxylic acid) and a six-membered ring (phenothiazine), despite some desulfurization during the baking process.

Smaller amounts of inorganic sulfides and sulfates are also found to exist in petroleum cokes.

Coal tar pitch is a byproduct of metallurgical coke production. Coal is heated in the coking oven, and the resulting product, coal tar, is collected and distilled. Coal tar pitch remains behind after the distillation process. Sulfur is also very abundant in coal and present both in organic and inorganic forms. Inorganic compounds can be removed via physical methods, but it is impossible to remove organic sulfur because it is a part of the coal structure. Abundant literature on the characterization of the nature of organic sulfur found in coal exists [59-61].

Some desulfurization methods for anode production have been investigated by thermal calcination. Based on prior research [63-65], Barillon and Pinnon [62] concluded that:

a) the higher the sulfur concentration in coke, the easier its removal,

b) residual sulfur concentrations from different cokes were fairly similar after heat treatment at over 1400 °C, and

c) any loss of sulfur resulted in changes to the structure of the coke (coke porosity increased and apparent density was reduced).

Jones et al [66] found that the removal of sulfur by thermal treatment (calcination) is impractical because rapid desulfurization did not occur until temperatures of around 1500 °C. Such an increase in anode calcination temperature would cause overcalcination for optimum anode and energy usage. Sulfur is therefore an inevitable impurity in aluminum anodes until a brand new removal process is found.

Sulfur that originates from alumina and fluoride additions is typically in sulfate forms [12]. Possible reactions of sodium sulfate with electrolyte taken from literature [67, 88, 91] are summarized in **Table 2.5**.

Table 2.5: Summary of possible reactions of sodium sulfate in cryolite melts at 980 °C [67, 88, 91]. Gibbs free energies for the reactions were calculated using HSC 7.1 software.

Na_2SO_4+C, CO	$\Delta_rG°$ (kJ/mol)	
$3Na_2SO_4 + 12C = 3Na_2S + 12CO$	-877	(2.32)
$3Na_2SO_4+3C = 3Na_2S+6CO_2$	-581	(2.33)
$3Na_2SO_4 + 2Na_3AlF_6 + 3C = 12NaF + Al_2O_3 + 3SO_2 + 3CO$	-209	(2.34)
$3Na_2SO_4 + 2Na_3AlF_6 + 3/2C = 12NaF +1.5CO_2 +Al_2O_3 +3SO_2$	-135	(2.35)
Na_2SO_4+Al		
$3Na_2SO_4 + 8Al = 4Al_2O_3 + 3Na_2S$	-3315	(2.36)
$3Na_2SO_4 + 2AlF_3 + 8Al = 6NaF + 4Al_2O_3 + Al_2S_3$	-3286	(2.37)
$3Na_2SO4 + 8Al = 3Na_2O + 3Al_2O_3 + Al_2S_3$	-2431	(2.38)
$3Na_2SO_4 +2Na_3AlF_6 +8Al = 12 NaF + 4 Al_2O_3 +Al_2S_3$	-3059	(2.39)

Burnakin et al. [67] noted that sulfate was moderately stable in cryolite melts without aluminum. Liquidus temperature of the electrolyte with additions of sodium and aluminum sulfate and sulfides was studied by recording cooling curves of the melt. Crystallization temperature decreased with sodium sulfate addition, and the effect was strongly marked in the presence of aluminum. The same effect was not observed upon sulfide (Na_2S, Al_2S_3) addition.

Grjotheim et al. [68] and several other researchers [69-72] also attempted to study the stability and phase diagrams of sulfates in cryolite melts. According to the results, there are broad ranges of solid solutions of sodium sulfate in the cryolite. Sodium sulfate was found to lower the crystallization temperature of cryolite and the solubility of alumina in the melt.

Sulfur is not known to accumulate in the bath. Instead, most of it is released as sulfurous gas emissions. Sulfur emissions from an aluminum smelter with an annual production of 200000 tonnes can be as high as 1000 tonnes of sulfur per year [73]. The most important reported sulfurous gases from aluminum reduction cells are SO_2, COS, H_2S, and CS_2. Sulfurous gases are known for their detrimental effect on local air quality (particulate matter), acid rain, human health, and global climate. It has been reported that particulate matter is a key ingredient of polluted air and has been estimated to kill more than 500000 people each year [74]. However, emission of sodium sulfide and conversion into sulfate are also argued to be the most important factors in lessening the warming of the earth by backscattering solar radiation into space [75]. A summary of reported average emissions of sulfur-containing gas species from different studies is given in **Table 2.6**.

Table 2.6: Average industrial emissions of sulfur containing gases.

Study	S in anode	Average SO_2	Average COS	Average H_2S	Average CS_2
	%	kg/t Al	kg/t Al	kg/t Al	kg/t Al
Tveito et al.[76][1]	1.4	1.5	0.65	0.2	-
Utne et al. [77][1]	1.1	2.32	0.28	-	-
Kimerle et al.[78]	2.4	24.8	1.1	-	-
Harnish et al.[79][2]	1.1	10	1.6	-	0.03
Global averages [79]	-	18	4	-	0.2

A number of theoretical and experimental studies was performed [76-82] to understand the formation of sulfurous gases. COS has been established as a dominant gas species. It is formed at the anode surface during electrolysis, and a large fraction is later oxidized to SO_2. Some of the findings of these studies are discussed below.

[1] after wet scrubber

[2] after electrostatic precipitators

The first study of sulfurous gas products from aluminum smelting was reported by Henry and Holliday [80]. Anode gas samples were taken from both prebaked and Söderberg cells. The primary sulfur compound detected was carbonyl sulfide, COS. A large amount of CS_2 was also observed during anode effects. Formation of COS is explained as a result of reactions between carbon, oxygen, and sulfur (or compounds containing these elements) at high temperatures:

$$CO + S = COS \quad (2.40)$$

$$CO_2 + CS_2 = 2COS \quad (2.41)$$

Sulfur dioxide is formed by oxidation of COS and CS_2. Reaction 2.40 should favor COS formation during normal operation because the amount of CO_2 is high at the anode. During anode effects, CO_2 content decreases, which should favor CS_2 formation. Particulate matter collected in the absence of air revealed the presence of elemental sulfur, suggesting the existence of red-ox reactions.

Oedegard [81] studied evolved gases from anodes containing 1-2 wt% sulfur during laboratory electrolysis experiments. Anode gases were sampled under inert conditions and analyzed by gas chromatography. COS was the major sulfur-containing compound detected. Dorreen [82] also found that COS was the main sulfurous gas formed in laboratory cells under inert conditions. He explained COS formation by the following reactions:

$$S + CO_2 + C = COS + CO \quad (2.42)$$

$$S + CO = COS \quad (2.43)$$

COS can also be produced electrochemically at potentials lower than that for Reaction (2.1) at 970 °C [82]:

$$Al_2O_3 + 3C + 3S = 3COS + 2Al \quad (2.44)$$

According to Reaction (2.44), carbon consumption can increase by 1.9% because sulfur has higher atomic weight than carbon and COS is formed [82].

Sulfur dioxide is formed by oxidation of COS via the following reactions [77]:

$$COS + 3/2O_2 = CO_2 + SO_2 \quad (2.45)$$

$$COS + 2CO_2 = CO + SO_2 \quad (2.46)$$

According to the above equilibria, unburnt gas will favor COS formation and the presence of air will favor the formation of SO_2.

Kimmerle and Noel [78] performed mass balance for sulfur and carbon by measuring of the levels of CO_2, CO, COS, and CS_2 with gas chromatography. SO_2 was determined by ion chromatography (see **Table 2.7**). **Table 2.7** shows that sulfur does not accumulate in the bath, but leaves the cell in the form of sulfurous gases as the total input of sulfur (13.0±0.5 kg/ t Al) is equal to total output (13.1±1 kg/t Al).

Table 2.7: Mass balance of sulfur [78].

Input	%	kg/t Al	Emissions	ppmv	kg/t Al
Anodes	2.45±0.1	10.1	COS	6.4±0.8	0.6±0.07
Anode cover alumina	0.2	0.1	CS_2	0.13±0.02	0
Scrubber alumina	0.14	2.4	SO_2		12.5±1
Coke scrubber alumina	0.21	0.4			
Total		13.0±0.5	Total		13.1±1

According to the data, nearly 96% of sulfur is released as SO_2, and around 4% as COS. The authors concluded that COS levels do not follow a linear relationship with sulfur concentration in the anodes. The average amount of COS produced per each tonne of aluminum was 1.1 kg for anodes containing 2.4% sulfur. Nearly all generated COS gas leaves the cell through exhaust without appreciable oxidation. CS_2 goes through rapid oxidation as it passes through the hot air atmosphere. This is supported by calculated negative values of Gibbs free energies for 100 and 1000 °C. The authors offered the above explanation for varying CS_2 concentrations observed at the anode, in the cell, and in the cell exhaust gases.

$$CS_2 + 3O_2 = CO_2 + 2SO_2 \quad (2.47)$$

$$CS_2 + 5/2O_2 = CO + 2SO_2 \quad (2.48)$$

$$CS_2 + CO_2 = 2COS \quad (2.49)$$

Oedegard [81] and Dorreen [82] used thermodynamic calculations to predict the composition of sulfurous gases. According to Oedegard [81], very little CS_2 should be present in the anode gas. COS is the most abundant gas species at low CO_2/CO ratios while SO_2 dominates at high CO_2/CO ratios.

Dorreen's thermodynamic predictions concluded that COS was the dominant gas formed at the anode surface both in laboratory and industrial cells when the gas was unburnt. When the gas was partially burned, the CO_2/CO ratio increased and the amounts of S_2 and SO_2 increased marginally. Totally burned gas contained CO_2 as the main gas component with SO_2 being the major sulfur-containing gas. Dorreen [82] supported his results with laboratory measurements. Thermodynamic calculations explain why only COS was observed in laboratory cells, where no oxidizing conditions exist to form SO_2. The absence of S_2 and CS_2 was attributed to possible reactions with alumina used as a dry-scrubber in the experimental set-up. A later study by Tveito et al. [76] showed that CS_2 is completely adsorbed in the dry scrubber. Some SO_2 is also adsorbed, and COS and H_2S show very little adsorption.

Hay [55] used HSC software to calculate the relative composition of sulfur species at equilibrium at the anode and in the cell hooding. Calculated results agree with previous findings that COS formation at the anode can be predicted from thermodynamic calculations.

Burnakin et al. [83] performed an overvoltage study utilizing anodes with varying concentrations of sulfur ranging from 0.94 to 2.52 wt%. Overvoltage decreased by 38.2 mV per 1 wt% of sulfur concentration in the anode for current densities in the range of 0.1-0.7 A/cm^2. Based on these results, it was concluded that thiophenes participate in the electrode process, and their oxidation leads to anode depolarization. The same effect was not observed at higher current densities. Potential theoretical reactions for this process are:

$$4Al_2O_3 + C_4H_4S = 8Al + 4CO_2 + SO_2 + 2H_2O \quad (2.50)$$

$$2Al_2O_3 + C_4H_4S = 4Al + S + 4CO + 2H_2O \quad (2.51)$$

$$3Al_2O_3 + C_4H_4S = 6Al + COS + 3CO_2 + 4H_2O \quad (2.52)$$

$$3Al_2O_3 + C_4H_4S = 6Al + CH_4 + 3CO_2 + SO_3 \quad (2.53)$$

$$3Al_2O_3 + C_4H_4S = 6Al + 4CO + SO_3 + 2H_2O \quad (2.54)$$

Thorne et al. [84, 85] also investigated overvoltage with increased levels of sulfur in the anode and reported that overvoltage is reduced at higher impurity levels. The authors also noted that overvoltage correlated with isotropy and oxygen content. It was therefore not conclusive, which effect was observed.

Burnakin et al. [86] made measurements on resistivity of baked anode mass and found that an increase in sulfur content in the anode by 1 wt% led to an increase in ohmic resistivity by 12%. This can increase specific energy consumption by approximately 200 kWh/t Al when anodes containing 1.5 wt% of sulfur are utilized.

In a subsequent study [67, 87], the same authors investigated the behavior of sulfur ions in cryolite melts by adding sodium sulfate. Sulfates were found to influence anodic overvoltage, liquidus temperature, and aluminum loss. A striking drop in anodic overvoltage was observed when 2.5% of sodium sulfate was added. as the authors proposed that the drop was a result of involvement of sodium sulfate in anode Reactions (2.35) and (2.36). Since the effect on overvoltage remained present even though sulfate concentration decreased, it was suggested that sulfide can be oxidized at the anode. The estimated current efficiency reduction due to an increase in concentration of sodium sulfate up to 3 wt% was between 0.2-0.3%. Observed loss of aluminum was attributed to possible reactions between sodium sulfate and aluminum (Reactions 2.36-2.39). Baimakov and Vetyukov [88] also discussed the possibility of sodium sulfate reacting with aluminum according to Reaction (2.36), forming sulfides that will be oxidized at the anode to SO_2:

$$S^{2-} + 2e^- = S \tag{2.55}$$

$$S + 2CO_2 = SO_2 + 2CO \tag{2.56}$$

Fellner et al. [89, 90] studied the reactions of sulfides with metal oxides (FeO, NiO). These reactions resulted in the formation of insoluble products (FeS, NiS). Al_2S_3 itself was found to be readily soluble in cryolite melts.

Ambrova and co-workers performed an extensive study of sodium sulfate behavior in sodium chloride and sodium fluoride melts [91-94]. They deduced that the kinetics of the chemical reactions in cryolite melts were similar to those in sodium chloride and sodium fluoride melts. Sodium sulfate can be reduced to sulfides in the presence of carbon and aluminum. This was confirmed by bath analysis, which detected Na_2S, Al_2S_3, and polysulfides.

According to Hajasova [73], electrochemical behavior of sulfate anions is not the same in chloride and fluoride melts. The electrochemical behavior of sulfate anions was studied by cyclic voltammetry, chronoamperometry, and square wave voltammetry. The most suitable working electrodes were platinum for chloride melts and gold for fluoride melts. It appeared that sulfate reduction involved more electrons in fluoride than in chloride melts. It was proposed that sulfate ions behave differently in electrolytes with different compositions. Temperature differences between experiments were too small to cause the observed differences in sulfate ion behavior. Experiments were run for four different cryolite ratios (mol NaF/mol AlF_3): 1.2, 1.5, 2, and 3. Cryolite ratios equal to 1.2 and 1.5 are not common bath compositions in the aluminum industry. However, low cryolite ratios may be utilized in the future if inert anodes are implemented.

Hajasova [24], with reference to Castro [95], discussed the instability of sodium sulfate above 900 °C. She presented a scheme of thermal stability of sulfur containing species. The scheme is illustrated in **Figure 2.2**. According to the scheme, if sodium sulfate is transformed into sodium sulfite, it will decompose further to sodium sulfate

and sodium sulfide. Sodium sulfate itself will decompose to Na_2O and SO_3. SO_3 is unstable above 778 °C and will further decompose to oxygen and sulfur dioxide.

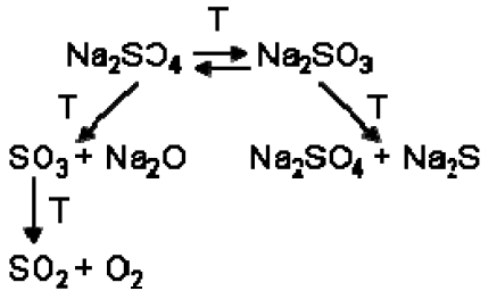

Figure 2.2: Scheme of thermal stability of sodium sulfate where T represents temperature [24]

Hajasova [73] also proposed a possible sulfate reduction mechanism based on the number of electrons found from prior measurements:

$$2SO_4^{2-} + 3e^- = S_2O_4^{2-} + 4O^{2-} \quad (2.57)$$

$$S_2O_4^{2-} + 2e^- = S_2O + 3O^{2-} \quad (2.58)$$

S_2O can only exist as an intermediate. It is an unstable compound and will decompose to SO_2 and S°.

The effect of sulfur concentration on carbon consumption was also of interest for many researchers, therefore broad literature exists [7-8, 96-101]. Theoretical carbon consumption as calculated by Faraday's law is 0.334 kg/kg Al according to Reaction (2.1). The other side reactions that can cause extra carbon consumption are: oxidation in the air (air reactivity), the back reaction, the Boudouard reaction (carboxy reactivity), and sulfur reactions. Excess carbon consumption by oxidation in the air and the Boudouard reaction can be catalyzed by many impurities causing extra carbon consumption (0.02 to 0.15 kg C/kg Al) [96].

Sulfur has been claimed to inhibit carbon consumption because it belongs to the group of halogens that accept electrons [7]. Electron acceptors form negative ions at the carbon surface and increase the energy barrier for oxygen chemisorption. As such, they can inhibit oxidation of the anode. Another possibility is that sulfur can form sulfides with major impurities found in carbon anodes, which, as a result, retards their catalytic effect. Eidet et al. [8] reported that sulfur alone had no significant effect on air and carboxy reactivity, but sulfur reduced the effect of iron catalysts to air reactivity. In another study, Eidet et al. [97] found that sulfur hindered the effect of vanadium on the carboxy reaction. On the other hand, Aanvik et al. [98] reported that an addition of 1 wt% sulfur to cokes had no apparent effect on either carboxy or air reactivity, hence no affect at all on carbon consumption. Another study found that sulfur can inhibit the catalytic effect of Na by forming a bond with Na [9]. Bensah et al. [99] suggested that 1-butanethiol could be a possible organic sulfur compound that

retards the effect of sodium. Xiao et al. [100, 101] claimed that sulfur has a significant catalytic effect on both air and carboxy reactivity when there is no intervention from other impurities. When calcium was added, sulfur and calcium were found to restrain each other's catalytic properties.

The discrepancies in the above papers can be explained by differences in sample preparation methods. Some researchers used artificially doped cokes, whereas others used cokes with naturally varying sulfur levels. It is hard to tell which method is best as artificially doped impurities may not behave in a similar way as in natural cokes. However, the effect found in natural cokes might not be attributable only to sulfur because those cokes contain other impurities too [5]. Moreover, it is known that low sulfur cokes and high sulfur cokes have different structures and densities, which can both affect carbon reactivity [66].

Earlier studies on current efficiency are contradictory. Bullough and Marshall [103], with the reference to Pearson [104], attempted to find the magnitude of current efficiency reduction by using prebaked anodes (0.8-1.6 wt% S) in a 10 kA reduction cell on small scale test equipment. Plant correlation of sulfur data with current efficiency recordings over a long period of time was also given. The reported current efficiency reduction was 5 ± 2% per each percent in sulfur increase. The authors commented that the observed current efficiency reduction should be due to a change in sulfur concentration in the anode as other tests with different vanadium content but similar sulfur content did not show any change in current efficiency. Later Barillon and Pinoir [62] investigated the behavior of prebaked anodes with sulfur contents of 1-3.5 wt% in industrial cells operated for long periods of time. They observed a slight effect of sulfur on current efficiency reduction, concluding that even a substantial increase in anode sulfur has no effect on current efficiencies observed on either industrial or laboratory scale. Gilmore and Bullough [10] also confirmed that there was no sulfur effect on either current efficiency or metal quality in industrial or laboratory tests.

LaCamera et al. [105] studied the behavior of sulfur in inert anodes. They reported that sulfur can build up in a cell using inert anodes and reach levels above 500 ppm and often even above 1000 ppm. These high levels may have been caused by the addition of raw materials such as alumina and aluminum fluoride, which can contain sulfur. Inert anodes do not produce CO_2, but evolve oxygen. This is not a problem in Hall-Héroult cells because sulfur impurities are removed by consumable carbon anodes, which produce COS or other sulfur containing gas species. Sulfur species have high solubility in the bath and can thus act as oxidizing agents to react with Al forming Al_2O_3. This may reduce current efficiency due to the undesirable back reaction. Sulfur can be present in the bath in various oxidation states: S(-2), S(0), S(+2), S(+4), and S(+6). The latter is more disadvantageous in inert anodes as it can be easily reduced and subsequently reoxidized. Like phosphorus, sulfur impurities may undergo cyclic red-ox reactions, consuming electric current that would otherwise be used for aluminum electrolysis. Moreover, sulfur impurities have a negative effect on interfacial energy between the bath and the aluminum pad. This can cause uncoalesced aluminum to disperse into the bath, where it can be easily

oxidized. Sulfur levels above 500 ppm were found to reduce current efficiency from 92-96% to 80% and below [105]. The effect was more pronounced when sulfur and iron impurities were present simultaneously [105]. The build-up of sulfur and iron in the bath can also result in the removal of produced aluminum.

Recent work that motivated the current study was reported by Pietrzyk and Thonstad [11], who performed laboratory studies on anodes containing sulfur in the range of 0 to 3.8 wt%. They claimed that sulfur has a negative effect on current efficiency. Graphite anodes were used as a zero sulfur carbon material, and prebaked anode samples supplied from industry had sulfur contents ranging from 2 to 3.8 wt%. The results of the current efficiency studies are shown in **Figure 2.3**. Current efficiency was determined by two methods: weighing the amount of deposited aluminum and oxygen balance. The authors observed a decrease in current efficiency, independent of the method used for its determination. Current efficiency was reduced by 1.8% per 1 wt% of sulfur in the anode for the aluminum weight method. The other method revealed a reduction by 1.6% per 1 wt%. Carbon consumption increased by 5.2% per 1 wt% of sulfur in the anode. However, a comment was made that the determination of carbon consumption by direct comparison of graphite anodes with prebaked anodes might not be a reliable approach. If the data from graphite anodes were excluded, carbon consumption did not change significantly. In the case of current efficiency, the authors argued that graphite data are relevant because the back reaction is not a part of the anode reaction.

Although extensive research has been done to study sulfur impurities, only a few studies focused on the effect of sulfur on current efficiency and the results are ambiguous. While sulfur does not accumulate in the bath, it can be present at low levels of up to 200 ppm [106]. If sulfur undergoes cyclic red-ox reactions as phosphorus does, even such a low concentration might have a significant impact on cell operation.

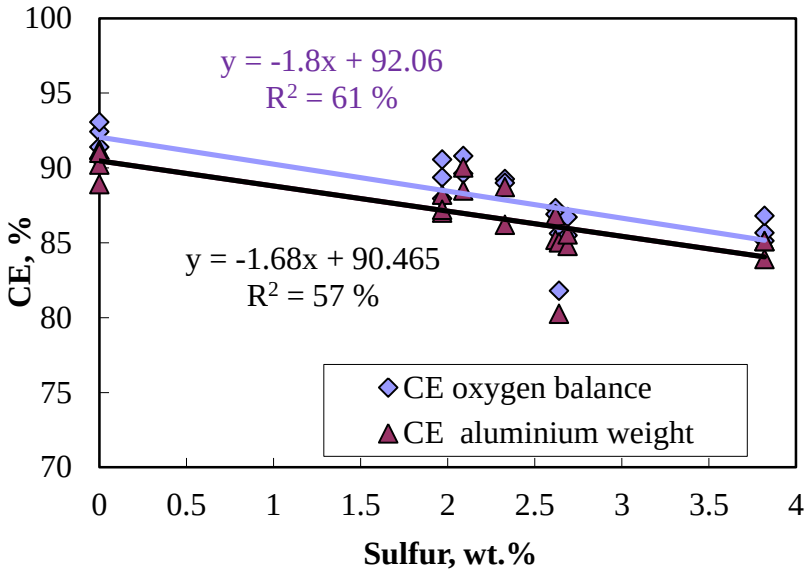

Figure 2.3: Influence of anode sulfur content on current efficiency (CE) [11].

3 EXPERIMENTAL

3.1 Methodology and Experimental Set-Up (Supplements 1, 2, 3 & 5)

3.1.1 Choice of Cell Design

The experiments in *Supplements 1, 2, 3, and 5* were carried out in a laboratory cell. The schematic of the cell design is given in **Figure 3.1**. The industrial cell represents a complex system where all parameters are closely interrelated. This makes it difficult to change a single parameter independently. Previous studies [12, 14] reported that various parameters such as temperature, cryolite ratio, bath additives, cathodic current density, and mass transfer coefficient influence current efficiency. Laboratory studies offer the possibility to change one parameter at a time, so direct effects of individual parameters can be determined. In addition, there is no need for the frozen sideledge, which makes it easy to carry out experiments at higher current densities.

The only drawback to performing experiments in laboratory cells is the difficulty of obtaining similar convective patterns as in industrial cells. Cell convection plays a big role in mass transport. Increased convection in the electrolyte reduces diffusion layer thickness, which in return increases mass transfer rate. Mass transfer of dissolved metal (Al, Na) through the diffusion layer near the cathode is the rate-limiting step in the back reaction [14]. Thus, the stability of the cell is imperative. It is likewise crucial to maintain an even current distribution by using suitable cathode material with good wetting properties towards aluminum. Otherwise, the deposited aluminum will have a hemispherical or spherical shape, which may not be representative due to the decreased current density at the sides of the sphere [1, 2].

Solli [2] developed a special laboratory cell to study current efficiency. The cathode in the cell is a stainless steel plate; this helps to maintain a sufficiently flat cathode. The anode is designed so that it gives efficient gas bubble release. The cathodic current density thus stays constant and is evenly distributed. This is important for current efficiency studies because current efficiency is a function of cathodic current density. Our work utilized this cell design to study the effect of impurities on current efficiency.

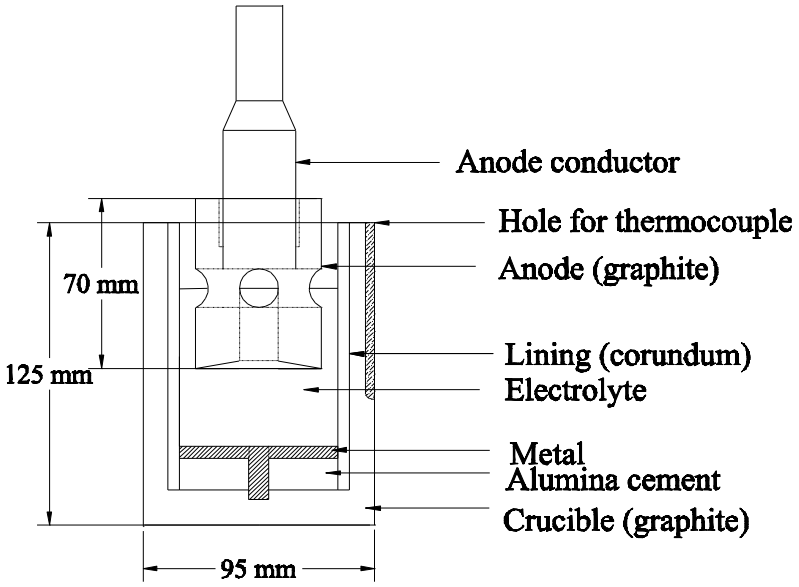

Figure 3.1: Schematic of the laboratory cell used for experiments described in *Supplements 1, 2, 3, and 5*.

3.1.2 Materials

Figure 3.2 and **3.3** show schematic illustrations of the anode design and anode conductor, respectively. The anode conductor was connected to the graphite anode. The anode is designed with vertical holes and horizontal channels to facilitate convection within the cell. The bottom of the anode has a 10-degree upward incline towards the center hole. Gas bubbles are thus expected to move towards the center hole of the anode and leave through the horizontal channels. A photograph of the anode is provided in **Figure 3.4.**

The list of materials and chemicals with information on suppliers is presented in **Table 3.1** and **Table 3.2**. With the exception of the anode conductor, the mullite (Pythagoras) tube, and the furnace components, all new components were utilized for every experiment to avoid carry-over from previous tests.

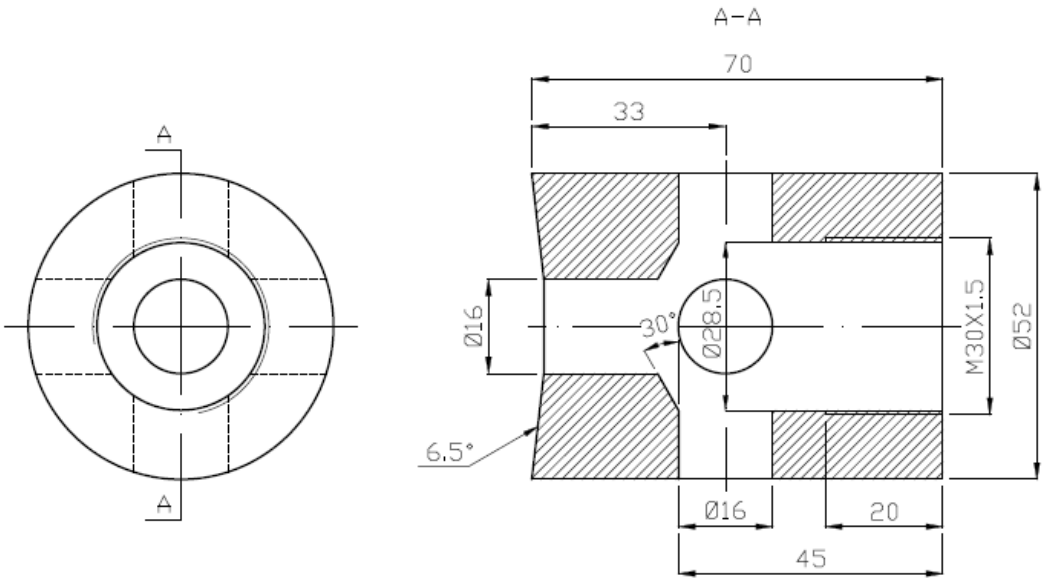

Figure 3.2: Graphite anode (sketch by Aksel Alstad, Date: 20141217).

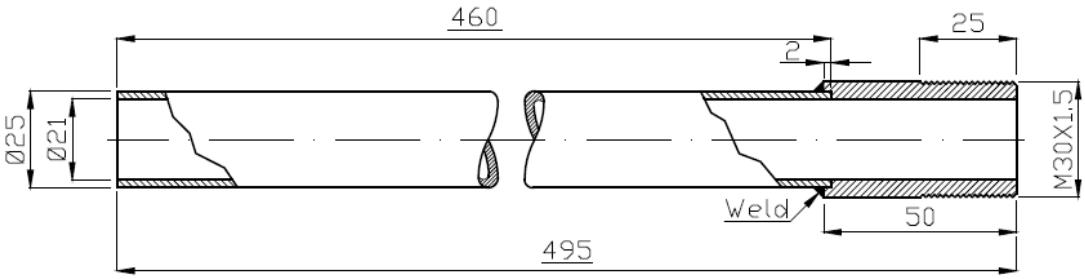

Figure 3.3: Anode conductor (sketch by Aksel Alstad, Date: 20141212).

Figure 3.4: Graphite anodes. Left: new anode; right: used anode after an experiment The photo was taken from the bottom of the anode, so the 10° inclination can be seen.

Table 3.1: List of materials and the suppliers, all dimension units are given in mm.

Material	Size	Suppliers
Graphite Anode	Ø52 x 70	Svensk Specialgrafit
Alumina lining, Alsint 99.7	Ø65 x 110	W.Haldenwanger
Stainless steel plate	Ø8 x 4	NTNU workshop
Stainless steel pin	Ø8 x 4	NTNU workshop
Graphite crucible	Ø95/76.5 x 126/110	Svensk Specialgrafit
Thermocouple tubes, Alsint 99.7	3 x 0.8 x 500; 8 x 5 x 500	W.Haldenwanger
Thermocouple wires, 10 %Rh/Pt		Johnson Matthey
Cement, 96 wt% of Al_2O_3 and 3 wt%		Borgestad Fabrikker
Nitrogen, 99.999 %		AGA

Table 3.2: List of chemicals used in this study.

Chemical	Suppliers
Na_3AlF_6 (heated at 200 °C for 24 h)	Hand picked, Øresund Greenland
AlF_3 (was sublimed at 1000 °C for 24 h)	Industrial grade, Alcoa Norway
Al_2O_3 (heated at 200 °C for 24 h)	Merck
$AlPO_4$ (heated at 200 °C for 24 h)	Merck
Na_2SO_4 (heated at 200 °C for 24 h)	Merck

3.1.3 Procedure

All the pins and stainless steel plates were weighed, labeled.. One pin was then placed into the hole inside a graphite crucible. Next, a sintered alumina cylinder was placed inside the crucible. The pin helps to provide electrical contact between the steel cathode and the graphite crucible. The bottom of the crucible was cemented with cast alumina cement (containing 96 wt% of alumina and 3 wt% CaO) as shown in **Figure 3.5**. Optimal cement layer was found to be 7 mm. A thinner cement layer could not hold the pin and alumina lining. Layers thicker than 7 mm did not leave enough space for the alumina powder. The crucibles with cement were allowed to dry at room temperature for 1-2 days followed by drying at 200 °C for two more days. If the crucible with wet cement was placed straight into the hot oven, rapid evaporation of moisture created undesired pores.

When the cement had dried, alumina powder was poured on top of it. These layers should prevent aluminum contact with the graphite crucible. Next, a steel plate was placed on top of the alumina powder. The stainless steel pin passed through all the layers and made contact with the steel plate. This pin provided contact with the current conductors leading current away from the cathode. Finally, the electrolyte mixture was poured on top of the steel plate. The electrolyte mixture was composed

of AlF_3 (25.2 g), Na_3AlF_3 (319 g), CaF_2 (18.92 g), and Al_2O_3 (15.13 g). This corresponds to a cryolite ratio of 2.5, with excess amounts of AlF_3, Al_2O_3, and CaF_2 of 6.75 wt%, 4 wt%, and 5 wt%, respectively. The crucible with all its described contents was kept overnight inside an oven at 200 °C.

Figure 3.5: Cementing crucible with alumina lining and stainless steel pin inside.

Before placing a crucible into the furnace, all the components of the furnace were cleaned well. A mullite (Pythagoras) tube with open ends was placed inside the furnace. The Pythagoras tube was cleaned and inspected for cracks prior to use. The two ends of the Pythogaras tube were closed with copper lids. The cathode lead (a stainless steel rod) was passed through the lower lid. A cathode conductor was connected to the graphite support. The stainless steel rod was shielded with radiation shields to maintain an even temperature distribution during the experiment. Shields were not used on the anode conductor rod to avoid contamination of the electrolyte with possible loose materials.

The crucible with the electrolyte mixture was placed on top of the graphite support inside the Pythagoras tube. The ends of the Pythagoras tube were closed by lubricated lids sealed with rubber O-rings to ensure a gas-tight furnace.

The furnace has its own thermocouple, which is in direct contact with the Pythagoras tube. Another thermocouple used to obtain temperature readings during the experiment was placed inside a slot in the crucible. This thermocouple was made of platinum and platinum rhodium alloy (Pt10Rh) wires placed inside an alsint thermocouple protection tube with double bore tubing. The thermocouple was fitted inside a sintered alumina sheath, which was placed in the crucible slot. During the initial experiments, a third thermocouple was placed directly in the electrolyte. The temperature difference between the thermocouple inside the electrolyte and inside the crucible slot was found to be 4.5 ± 1.3 °C from four repeated tests. In the next experiments, only the thermocouple placed inside the crucible slot was used, and the temperature difference was corrected. This prolonged the life of the thermocouple and reduced experimental costs.

The furnace temperature was set to 980 °C for 4 hours to melt the electrolyte mixture. Nitrogen gas was flushed through with a flow rate of 0.2-0.3 dm^3/min to prevent air burn. After everything had melted, the experiment was ready for start. First, the contact point between the anode and the electrolyte was found by lowering the anode into the electrolyte. After the contact position was established, the anode was lowered an additional 2 cm, so the electrolyte height was in the middle of the horizontal anode holes. The experiment was then initiated by applying current of a magnitude calculated based on desired current density. Cathodic current density is calculated from the total current by dividing by the cross-sectional area of the sintered alumina lining using the inner radius (equal to 33.17 cm^2). Current, voltage, and temperature were recorded in 10-second intervals. During electrolysis, the furnace temperature was controlled to maintain a constant electrolyte temperature of 980 °C. Average standard deviation during the experiments was ±10 °C. Average standard deviation between experiments was ±1 °C.

Alumina additions were made manually through a hole in the anode conductor every 15 minutes. The amount fed was calculated from the amount of aluminum produced according to Faraday's law for the given time and current.

The duration of each experiment was set so that the same amount of aluminum was produced. At high current densities, experimental duration was thus shorter than at low current densities. The length of the experiment ranged from 2-4 hours. Even though Solli [2] did not observe any effect of anode cathode distance (ACD) on current efficiency, special care was taken to keep ACD above 20 mm since Rolseth [107] found that current efficiency was not affected by ACD down to 20 mm in laboratory cells. After each experiment, the crucible was broken and aluminum was cleaned mechanically and left in an aqueous solution of $AlCl_3 \cdot 6H_2O$ for 30 minutes. The metal was then cleaned again and left to dry inside an oven at 200 °C. Once the metal was dry, the weight of produced aluminum was determined by subtracting the pin and plate weights. Current efficiency was determined according to Equations (2.2) and (2.3). Estimated loss because of metal handling was assumed to be 0.9%, a value reported by Solli [2].

3.1.4 Choice of Method for Determination of Current Efficiency

Several methods to determine current efficiency exist. The most frequently used ones are: gas analysis of CO/CO_2 (Pearson and Waddington equation), total oxygen balance, weighing of the produced metal, and use of tracers. The use of trace metals is common for industrial experiments, but not for laboratory setups.

Determination of current efficiency by gas analysis of CO/CO_2 assumes that the main gas product is CO_2 due to the cell Reaction (2.1). CO originates from the back Reaction (2.2). Current efficiency can be estimated from the gas data by the Pearson-Waddington equation [14]:

$$CE\% = 100\% - 0.5\{\%CO_{(g)}\} = 50\% + 0.5\{\%CO_{2(g)}\} \quad (3.1)$$

The advantage of this method is that results can be obtained rapidly. The disadvantages are other factors that can contribute to changing the CO/CO_2 ratio. The

Boudouard reaction is an example. Another gas analysis method - total oxygen balance, where all the volume of the gas is analyzed for total oxygen content - has been proven to give more accurate results and eliminate the problems associated with the Pearson and Waddington method [14].

Due to the experimental set-up used in this study, gas analysis methods were not suitable. The anode conductor tube was opened every 15 minutes for alumina feedings. For the sulfur experiment, the tube was opened every 10 minutes. We chose to determine current efficiency from direct aluminum weight, due to both convenience and accuracy.

3.2 Methodology and Experimental Set-Up for Industry-Scale Experiments (Supplement 4)

Industry-scale experiments were conducted at the Alcoa Fjarðáal smelter in Reyðarfjörður, Iceland. Alcoa Fjarðáal is a point-fed prebaked smelter with 336 cells. The smelter was constructed in 2004-2007 and reached full capacity (346 000/year) in 2008 [108].

3.2.1 Data Analysis Methods

Data analysis was performed only for phosphorus because analysis of phosphorus concentration in the metal is completed routinely at the smelter. Measuring phosphorus content in the electrolyte is not a part of the routine, however. Phosphorus concentration in the bath can be estimated by applying a rule of thumb, where the relationship between electrolyte and metal concentrations of phosphorus is tenfold [30]. According to literature [1, 30], phosphorus deposition is mass transfer limited. When phosphorus concentration increases in the electrolyte, this will cause a corresponding increase in metal concentration.

Regression analysis was performed on phosphorus concentration in the metal and different process parameters recorded for the period from January 2011 to December 2013.

In order to construct trend plots, phosphorus concentration in the metal was divided into several categories: up to 4 ppm, 4-9 ppm, 9-14 ppm, and 14-20 ppm. In industry, phosphorus concentrations up to 4 ppm in the metalare considered low and do not present any harm; concentrations between 4-9 ppm are considered average, and concentration greater than 9 ppm in the metal are considered high. Error bars represent standard error of the mean, which is calculated from the following equation:

$$Standard\ error\ of\ the\ mean = \frac{\sigma}{\sqrt{N}} \tag{3.2}$$

where is the population standard deviation and N is the sample size.

3.2.2 Experimental Sampling Device

Finding a suitable sampling device for taking electrolyte samples from industrial cells is crucial since the electrolyte may contain carbon dust. Carbon dust usually accumulates on the surface of the electrolyte, and it can serve as a nucleation site for impurities [14]. The standard procedure for collecting electrolyte samples at the smelters is by means of an iron spatula. It is an easy and fast sampling technique, especially when a large sample is required for analytical assays. Alcoa Fjarðáal uses X-Ray Fluorescence (XRF) and X-Ray Diffraction (XRD) spectroscopy for analysis of electrolyte samples. Both techniques require sample weights of 20 grams.

For the purposes of this thesis, the sampling technique used by Rolseth [109] was adapted and tested at the smelter. **Figure 3.6** shows a photograph of the sampling device. The body of the sampling device consists of a cup with a lid and a height adjuster. The cup can be positioned at different heights by regulating the height adjuster. The sampling device is closed while entering into the electrolyte. The lid is then lifted for a few seconds to allow electrolyte to flow into the device. The lid is then quickly closed, and the sampling device is lifted out. A bath sample weight of up to 30 grams can be obtained. The sampling device was modified and made lighter (7.1 kg down to 3.3 kg). This made sample collection easier, allowed for more frequent sampling, and improved stability of the sampling device during sampling as it was less disturbed by magnetic fields. Sampling frequency was increased due to faster cooling compared to the former device design. The amount of sample collected was increased to 40 grams, which enabled duplicate sample analysis. The modified version of the device is shown in **Figure 3.7**.

Figure 3.6: Sampling device adapted from Rolseth.

Figure 3.7: Modified sampling device.

In order to test the modified sampling device, fifteen samples were taken from the same cell: 5 samples by the modified Rolseth sampling device and 10 random samples by the iron spatula. The photo of the prepared samples pressed into tablets is shown in **Figure 3.8**. The black samples are a result of the presence of carbon dust in the samples.

Figure 3.8: Electrolyte samples pressed into tablets for XRF analysis. First row-modified Rolseth device, second row-iron spatula and third row-iron spatula. The difference between the second and third row is the presence of carbon dust in the samples.

Table 3.3 and **3.4** show the results of XRF analysis for phosphorus and sulfur. According to the analysis, the concentration of phosphorus was unaffected by the sampling technique. The difference in phosphorus concentration observed by the two methods is within the standard deviation between samples (64.0 ± 4.2 ppm in case of the modified Rolseth design and 65.2 ± 5.0 ppm when using the iron spatula).

However, sulfur concentration changed considerably depending on the sampling technique. The average sulphur concentration in samples collected by the modified Rolseth design and by the iron spatula was 94.8 ± 11.0 ppm and 461.4 ± 370.2 ppm, respectively. The samples were analyzed for carbon content in an attempt to understand the observed discrepancy in sulfur concentrations between the samples from the same cell. The analysis confirmed that sulfur concentration is a function of the concentration of carbon dust particles in the electrolyte (**Figure 3.9**). This highlights the importance of the type of sampling device for correct interpretation of results.

Table 3.3: Average phosphorus concentration and standard deviation in samples collected by the two sampling methods. All values are given in ppm.

Sampling device	P, ppm
Mod. Rolseth Device	64.0±4.2
Iron Spatula	65.2±5.0

Table 3.4: Average sulfur concentration and standard deviation in samples collected by the two sampling methods. All values are given in ppm.

Sampling device	S, ppm
Mod. Rolseth Device	94.8±11.0
Iron Spatula	461.4±370.2

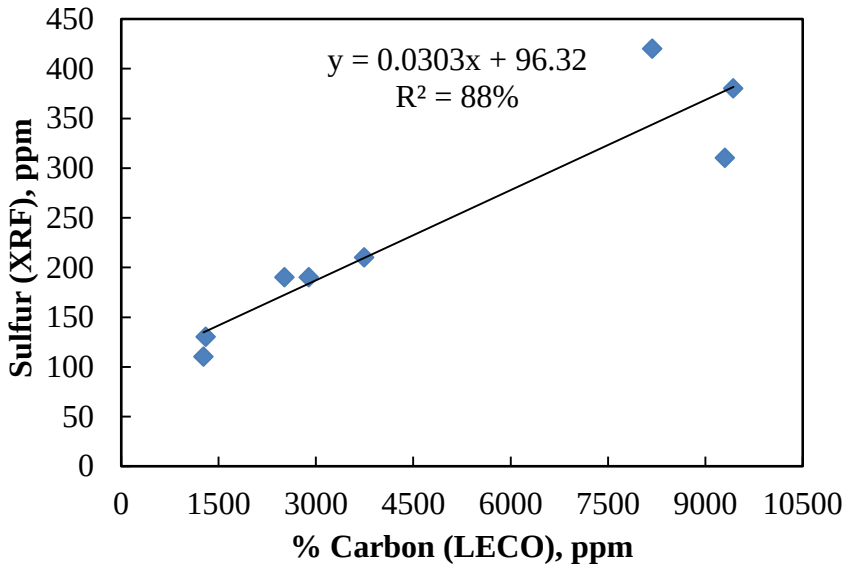

Figure 3.9: Sulfur concentration in the electrolyte (determined by XRF) as a function of carbon content in the electrolyte (determined by LECO).

3.2.3 Procedure

Procedures for pot selection were as follows: Data from the last three months were reviewed. First, pots that showed continuous high concentrations of phosphorus in the metal were selected. Next, pots with similar representative parameters such as temperature, age, bath ratio, base resistance, and noise were found. Lastly, preference was given to pots with the shortest physical distance from each other (this was done to ease workload when sampling).

Tests were started after metal tapping. Sampling was carried out during normal operation with the current at steady state at hourly intervals. During a controlled power cut, sampling was carried out at intervals of about 15-20 minutes. During the power cut, current was ramped down slowly to zero. One and a half hours later, the current was ramped up again step-by-step until full power was achieved.

Bath and metal samples were collected before, during, and after cutting the current. The samples were analyzed as a function of time. Bath samples were collected from the surface, middle, and close to the metal (end bath) by the sampling device described in section 3.2.2 and analyzed by XRF. The samples were additionally analyzed by XRD for excess AlF_3%, CaF_2, and alumina content. STARPROBE was used to record temperature and superheat change.

Metal samples were collected with a steel ladle. The samples were analyzed by Optical Emission Spectrograph.

3.3 Methodology and Experimental Set-Up for the Sulfur Experiment (Supplement 6)

3.3.1 Experimental Set-Up and Procedure

Experiments were run in the laboratory cell described in section 3.1.1 using the cryolite melt composition described in section 3.1.2. Sodium sulfate powder was pressed into tablets and added directly into the electrolyte during the experiments. Total sulfur amount in the electrolyte was measured by ICP-MS (Inductive Coupled Plasma-Mass Spectrometry). Electrolyte samples were taken at first every 5 minutes for 30 minutes. Samples were then taken every 10 minutes for another 30 minutes. After that the sampling frequency was 20 minutes for the duration of the experiment. Temperature was maintained at 980 °C. Experiments were run inside a gas-tight furnace flushed with nitrogen gas. The experimental scheme is outlined in **Table 3.5**.

Table 3.5: The experimental scheme. "C" is carbon, "Al" is aluminum, "El" is electrolysis, "S target" is the sulfur target added into the melt, "S melt" is the sulfur content in the melt at the beginning of the experiment determined by ICP-MS.

Test Name	Crucible	Time	C	Al	El	S target	S melt
		min				ppm	ppm
T1a	Alsint	0-120	-	-	-	1000	855
T1b	Alsint	120-180	+	-	-	-	624
T1c	Alsint	180-240	+	+	-	-	452
T2a	CE cell	0-120	+	-	-	1000	909
T2b	CE cell	120-180	+	+	+	-	136
T2c	CE cell	180-240	+	+	-	1000	1086
T3	CE cell	0-300	+	+	+	1000	836
T4	CE cell	0-280	+	+	+	500	573
T5	IndustrialCell	0-240	+	+	+	1000	724

The purpose of the T1 experiment were to investigate which gaseous compounds formed when reducing agents (C, Al) were introduced and to understand how the stability of sodium sulfate was affected. The molten electrolyte for this experiment was contained inside a corundum crucible. Sodium sulfate tablets with a target level of 0.44 wt% of sodium sulfate (1000 ppm sulfur) were added into the molten electrolyte at the beginning of the experiment.

Experiments T2, T3, and T4 were part of the study of the effect of sulfur on current efficiency. The current efficiency cell set-up shown in **Figure 3.1** was utilized. Sulfur stability and formed gas species were compared at different conditions, with and without imposed current.

Experiment T5 was performed in an industrial cell (A020 located at Alcoa Fjarðáal, Iceland) with prebaked anodes. The average electrolyte weight of the cell was assumed to be 7000 kg, and the required total amount of Na_2SO_4 added to the cell was 31 kg (7 kg of sulfur). Bags with sodium sulfate were carefully added through the tapping hole (located at the end of the cell) and through the central alumina feeding hole. Electrolyte samples were taken before and during the entire experiment. No gas measurements were performed during this test.

3.3.2 Gas Analysis Method

Furnace off-gases were passed through a mass spectrometer (MS) for qualitative assessment. MS was the only available gas analyzer when the experiments were performed. The drawback of the available equipment was inability to provide quantitative data. No mass balance of sulfur could thus be performed. The gas analysis results were used only to support other results and identify the gas products formed during the reactions.

3.4 Analytical Methods

Sulfur concentration can be determined by titrimetric analysis, LECO, XRF, XRD, ion chromatography, or ICP-MS. After many verification tests, ICP-MS and XRF showed the best reproducibility among these methods and were selected as our analytical methods. ICP-MS also has the lowest detection limit: 0.4 ppb for phosphorus and 20 ppb for sulfur. XRF has a detection limit of 15 ppm for phosphorus and 40 ppm for sulfur. All electrolyte samples from the laboratory tests were analyzed by ICP-MS. XRF was the available equipment at Alcoa Fjarðáal, and industrial electrolyte samples were therefore analyzed by XRF. Since the detection limit for sulfur with XRF is higher, a predetermined amount of sodium sulfate was mixed into the crushed electrolyte prior to sample analysis. The results confirmed that XRF is an accurate method for detecting sulfur content (**Figure 3.10**).

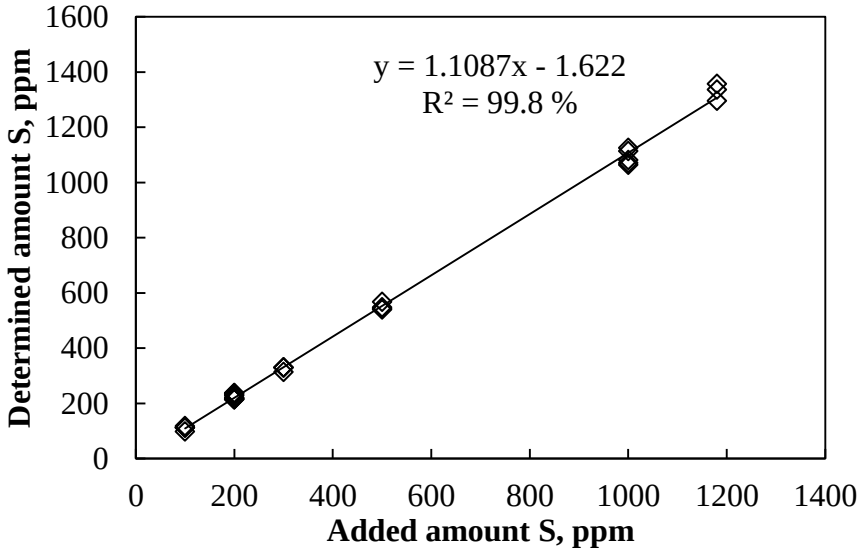

Figure 3.10: Comparison of added and analytically determined sulfur concentration.

4 RESULTS AND DISCUSSIONS

4.1 Laboratory Studies

4.1.1 Effect of Current Density on Current Efficiency (Supplements 1-3)

The influence of current density on current efficiency (CE) was studied first, prior to the study of the effect of impurities at high current density (1.5 A/cm^2). Figure 4.1 compares the results of CE as a function of current density from the present study with literature studies that used the same cell set-up [2, 109].

According to **Figure 4.1,** the present study is in good agreement with literature studies at similar current densities. However, Solli's [2] results show a maximum (94.1%) at 1.1 A/cm^2 compared to the present study, which shows a maximum (average 95.5%) at 1.5 A/cm^2.

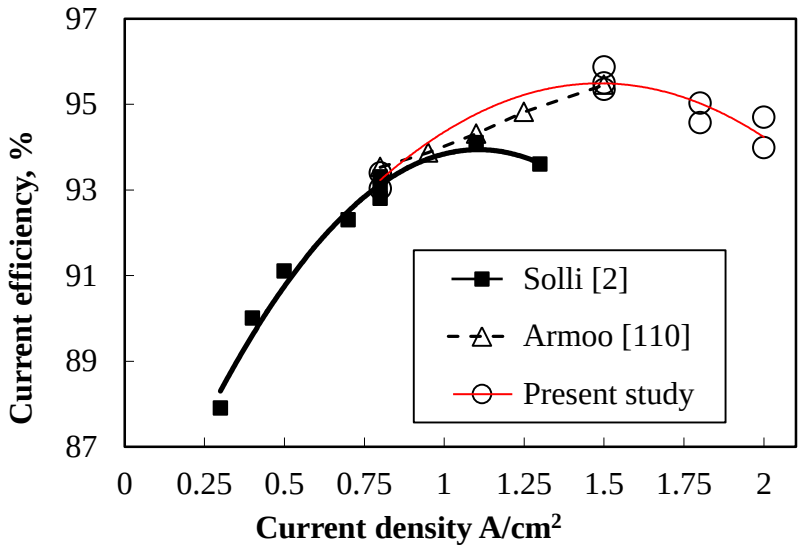

Figure 4.1: CE as a function of current density in molten Na_3AlF_6-Al_2O_3 (sat)-AlF_3 (7 wt%)-CaF_2 (5 wt%) at 980 °C.

If the current density change is compared with the rate of production (theoretical and actual), the rate of reoxidation (back reaction) and CE (**Figure 4.2** and **Table 4.1**), CE is seen to decline at high current densities despite a continuous increase in both theoretical and actual production rates. This behavior can be explained by two competing mechanisms taking place: an increased rate of metal production due to the increased total current (current density) and the rate of the back reaction. The rate of

the back reaction is controlled by mass transfer and should be independent of current density unless other conditions are changed.

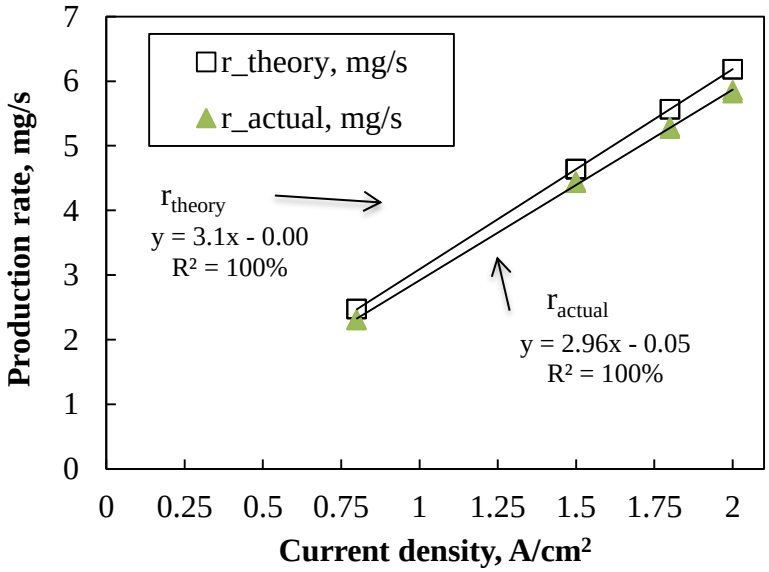

Figure 4.2: Theoretical rate of production (r_theory) and actual rate of production (r_actual) as a function of current density.

Nevertheless, the increase in current density causes an increased stirring effect in the melt due to fluid dynamics, enhanced gas evolution, and bubble formation. Magneto-hydrodynamics will also increase stirring as current density increases. Consequently, the boundary layer becomes thinner, which results in faster mass transfer and an increased rate of metal reoxidation. Polyakov [111] reported that interfacial stirring between electrolyte and metal can contribute to a decrease in CE. Haupin and McGrew [112] noticed an enlargement of gas bubble size with increased current density. In the present study, noise due to bubbling was more pronounced at cathodic densities ranging from 1.8 to 2 A/cm^2, suggesting the presence of larger gas bubbles at these densities.

The cryolite ratio (NaF/AlF_3) is also higher at the cathode when current density increases. This is due to enhanced migration of sodium ions, which act as current carriers [113]. A higher cryolite ratio at the cathode boundary layer will increase metal solubility [14] and in turn increase the rate of the back reaction.

The observed maximum CE at 1.5 A/cm^2 might not be the case for other cell set-up configurations with different flow patterns and different electrolyte compositions. However, the basic principles are expected to remain the same and a decrease in CE at very high current densities (above 1.5 A/cm^2) can be expected due to a higher rate of the back reaction caused by faster fluid flow and more efficient mass transfer.

Table 4.1: Rates of metal production and reoxidation increase as a function of current density. Here, r_{theory} is the theoretical rate of production, r_{actual} is the actual rate of production, $r_{reox.}$ is the rate of the reoxidation reaction.

CD	r_{theory}	r_{actual}	$r_{reox.}$	CE
A/cm^2	mg/s	mg/s	mg/s	%
0.8	2.474	2.323	0.151	93.9
0.8	2.474	2.311	0.163	93.4
0.8	2.474	2.301	0.172	93.0
1.5	4.639	4.447	0.192	95.9
1.5	4.639	4.430	0.209	95.5
1.5	4.639	4.423	0.216	95.4
1.8	5.566	5.290	0.277	95.0
1.8	5.566	5.264	0.302	94.6
2	6.185	5.858	0.328	94.7
2	6.185	5.814	0.372	94.0

4.1.2. Effect of Phosphorus on Current Efficiency

4.1.2.1 Phosphorus Concentration during the Experiments *(Supplement 3)*

To study the effect of phosphorus on CE, $AlPO_4$ was added directly into the electrolyte. Thisted [1] and Keppert [51] have used $AlPO_4$ in their studies of electrochemical behavior of phosphorus.

Initially, 10% of the phosphorus was added every 15 minutes with alumina feedings to maintain a constant phosphorus concentration. Later control studies, where electrolyte samples were collected during the experiment, revealed that this was unnecessary and led to phosphorus accumulation. The tests where the predetermined amount of phosphorus was added only once at the beginning of the experiment showed that phosphorus content in the electrolyte stays largely constant during electrolysis. **Figure 4.3** shows how phosphorus concentration changes over the course of four hours during electrolysis. The results contradict the statement that phosphorus compounds are volatile in aluminum reduction cells [43, 44]. On the contrary, the data suggest a long residence time probably due to cyclic redox reactions [30]. The observed initial loss and subsequent stability may indicate that phosphorus changed chemical forms (oxidation state) over time. The volatile form may not have been present after some initial time period. Haugland et al. [30] added phosphorus into industrial pots and found minimal phosphorus decay over time. Thisted [1] observed a maximum deficit of phosphorus in the electrolyte close to 70% due to inefficient addition through the anode conductor of the laboratory cell. However, the concentration of phosphorus stayed approximately constant during

electrolysis. In our study, phosphorus was added in advance into the electrolyte mixture to avoid inefficient addition. The phosphorus content dropped only minimally at the beginning of the electrolysis and stayed more or less constant throughout the following 4 hours (**Figure 4.3**).

Figure 4.4 was obtained by plotting average phosphorus concentration in the bath (from **Figure 4.3**) versus the added amount. It can be used to predict an expected steady-state concentration of phosphorus in the electrolyte for a known initial amount of added phosphorus.

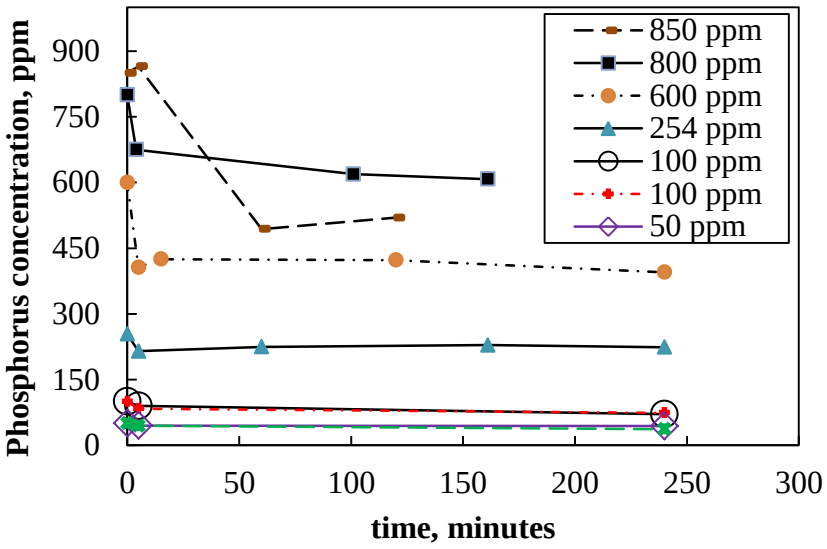

Figure 4.3: Changes in phosphorus concentration over time for different concentrations of phosphorus added at the beginning of the experiments.

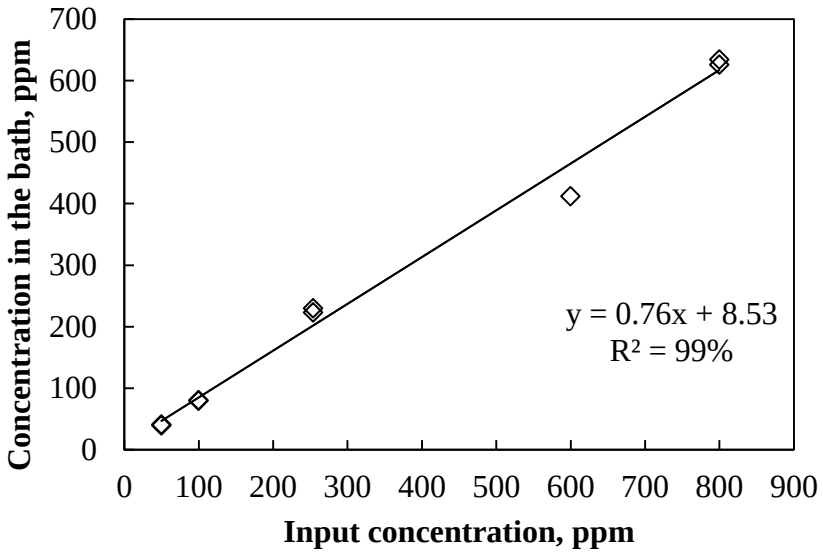

Figure 4.4: Average concentration of phosphorus in the bath analyzed by ICP for each phosphorus input concentration [114].

4.1.2.2 Effect of Phosphorus on Current Efficiency *(Supplement 3)*

The effect of phosphorus was first studied at current densities of 0.8 A/cm^2 as a control parameter. This was a repeat of previous works done by Thisted [1] and Solli [2], which used same current densities. Experiments were then performed at a higher current density of 1.5 A/cm^2. Other parameters were selected to match Thisted [1] and Solli [2]. Experimental methodology is provided in Chapter 3.1. The results of the present study on CE as a function of phosphorus content in the electrolyte are presented in **Figure 4.5**. Literature results are included for comparison.

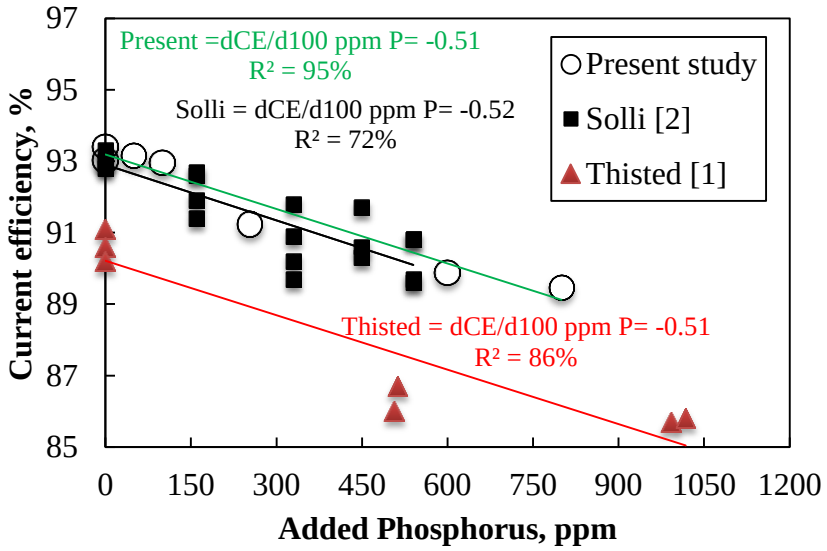

Figure 4.5: CE for aluminum deposition as a function of added phosphorus concentration in molten Na_3AlF_6-Al_2O_3 (sat)-AlF_3 (7 wt%)-CaF_2 (5 wt%) at 980 °C and at 0.8 A/cm^2.

As can be seen from **Figure 4.5**, the reported results for the present study are in agreement with the results obtained by Solli [2] and Thisted [1]. The CE reduction calculated for the present study is 0.51% ± 0.07 per 100 ppm of phosphorus increase at 0.8 A/cm^2. Thisted [1] and Solli [2] report CE reductions of 0.51% and 0.52% per 100 ppm of phosphorus, respectively. Both also reported that the effect of further phosphorus additions on CE is less pronounced at higher concentrations. Solli [2] observed a flattening of the CE curve at phosphorous concentrations higher than 330 ppm, while Thisted [1] saw a similar effect above 500 ppm. Both speculated that this could be due to higher evaporation of phosphorus compounds at these concentrations. **Figure 4.3** shows that at higher levels of phosphorus addition, the initial drop in concentration is greater when compared to lower concentration additions.

Thisted reported that the average concentration of phosphorus in the electrolyte was 300 and 400 ppm for the added amount of 500 and 1000 ppm, respectively.

Solli [2] did not measure phosphorus content in the electrolyte, but an expected concentration in the electrolyte can be estimated from **Figure 4.4**. **Figure 4.6** shows CE as a function of the average phosphorus content in the electrolyte. According to **Figure 4.6**, the effect of phosphorus given by Thisted is higher (1.3% per 100 ppm of phosphorus in the electrolyte) compared to the present study as well as to Solli [2], which are 0.67 and 0.68% respectively.

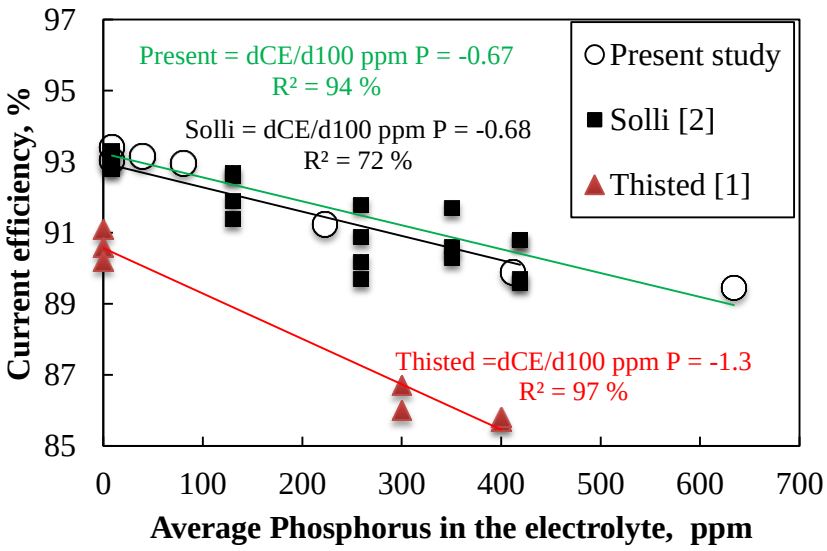

Figure 4.6: CE for aluminum deposition as a function of average phosphorus concentration in molten Na_3AlF_6-Al_2O_3 (sat)-AlF_3 (7 wt%)-CaF_2 (5 wt%) at 980 °C and at 0.8 A/cm^2.

The CE as a function of the average phosphorus concentration at 1.5 A/cm^2 is presented graphically in **Figure 4.7**. **Figure 4.7** includes data both from earlier experiments (*Supplements 1 and 2*) and later experiments (*Supplement 3*). The difference between them is that in earlier experiments ICP analysis of the electrolyte samples were not performed. They were corrected using **Figure 4.4**. Regression analysis of CE as a function of phosphorus content at levels of up to 630 ppm gives a reduction of 1.1% ± 0.21% per 100 ppm of phosphorus at 1.5 A/cm^2. This indicates a fallacy in the presumption that the effect of phosphorus might be less important at higher current densities. Instead, the results indicate that the effect of phosphorus is more pronounced at higher current densities. This can possibly be attributed to increased stirring due to bubble formation and fluid dynamic effects, which lead to thinner diffusion layers and therefore more efficient mass transfer to the reaction planes. Thus, cyclic redox reactions are enhanced at higher current densities. Another possibility is that, at high current densities, the higher cathode potentials push phosphorus to be reduced to lower oxidation states. Red-ox reactions with lower oxidation states can cause a larger CE loss due to the involvement of more electrons per cycle.

However, the concentration of phosphorus in industrial cells does not reach levels as high as 630 ppm. If the slope is calculated for CE decrease in the range of industrial interest (0-220 ppm), a reduction of 2.41% ± 0.45% per 100 ppm of phosphorus is obtained at 1.5 A/cm^2. Doing the same analysis for a lower current density (0.8 A/cm^2), a slope of 0.92% ± 0.16% per 100 ppm of phosphorus is found.

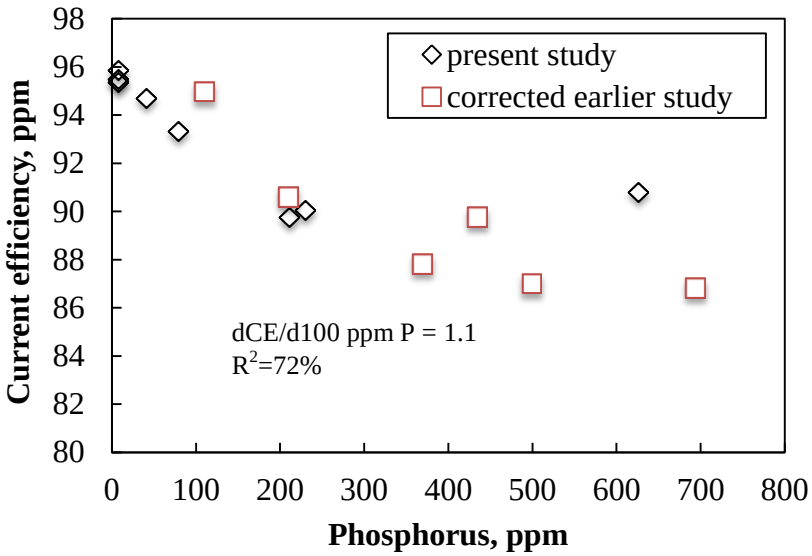

Figure 4.7: CE versus phosphorus concentration in the bath at 1.5 A /cm^2. Results from *Supplement 1 and 2* are shown in diamonds and results from *Supplement 3* are given in squares. Results from *Supplements 1 and 2* were corrected using **Figure 4.4**.

4.1.3 Effect of Sulfur on Current Efficiency

4.1.3.1 Sulfur Concentration during the Experiments *(Supplement 5)*

In order to investigate the effect of sulfur on CE, sodium sulfate was added directly into the electrolyte. Sodium sulfate should be stable in cryolite; several researchers have studied its stability and published phase diagrams of sulfate in cryolite melts [67-72]. Another option for sulfur addition would be to use anodes with different sulfur contents. This procedure would probably have made it easier to control sulfur concentration, but there are several drawbacks. High sulfur in the anodes is correlated with other trace impurities [66]. Anodes with different sulfur levels also differ not only in structure, but also in wetting properties and electrochemical behavior [84, 85]. Introduction of sulfur directly into the system can thus be an attractive alternative, but both strategies are helpful in elucidating the overall effects.

To find the amount of necessary sulfur compensation during the experiment, 0.44 wt% of sodium sulfate (1000 ppm sulfur) was added to the bath and sulfur concentration in the bath was measured over time. **Figure 4.8** shows that sulfur concentration decays rapidly after addition. Electrolyte samples were analyzed using ICP-MS (Inductive Coupled Plasma Mass Spectrometry). Retention time for sulfur in

the electrolyte follows an exponential function, as evidenced by a straight line on the plot of sulfur concentration on a natural logarithmic scale (**Figure 4.9**). Based on Figure 4.9, a linear regression of the data results in the following relationship for the decay of 1000 ppm of sulfur (:):

$$\mathrm{Ln}(C_S) = -0.1t + 7.3 \tag{4.1}$$

$$t_{1/2} = \frac{Ln2}{0.101} = 6.86\,min \tag{4.2}$$

Where C_s is the concentration of sulfur, t is the time of sulfur addition, and $t_{1/2}$ is half-life time.

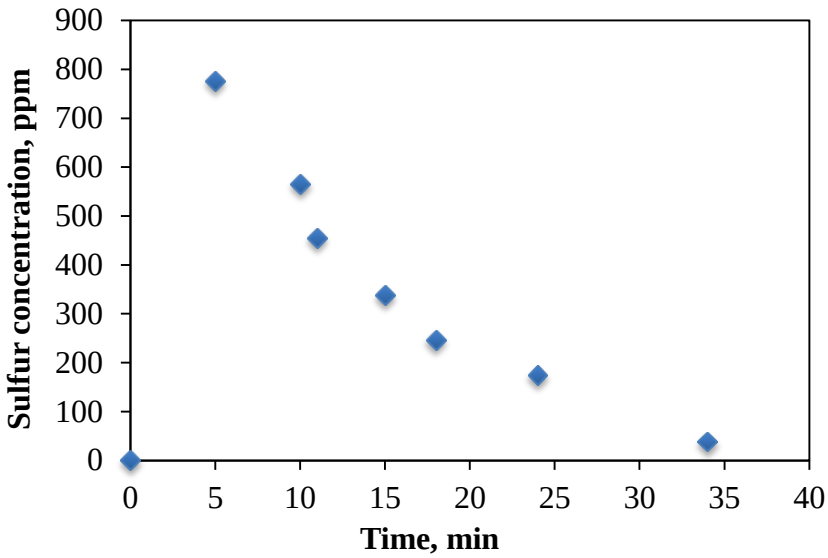

Figure 4.8: Sulfur concentration in the electrolyte over time [115].

Sulfur additions in the form of sodium sulfate tablets were made every 10 minutes. In order to check if feeding half of the initial amount of sulfur every 10 minutes to compensate for the sulfur loss was accurate, electrolyte samples were taken 5 and 10 minutes after each tablet addition. An attempt was made to collect electrolyte samples earlier than 5 minutes after addition, but these samples contained undissolved tablet residue. Sulfur concentrations obtained by ICP analysis were therefore significantly higher than expected (5000 mg/kg (ppm) versus 1000 mg/kg (ppm) of added sulfur), and the samples were not representative of the average sulfur concentration in the electrolyte. Samples taken 5 minutes post addition were free of tablet residue and indicate the maximum concentration of sulfur reached. Samples collected 10 minutes after tablet addition yield the lowest sulfur concentration. From these data, the possible occurrence of sulfur overfeeding or underfeeding can be determined.

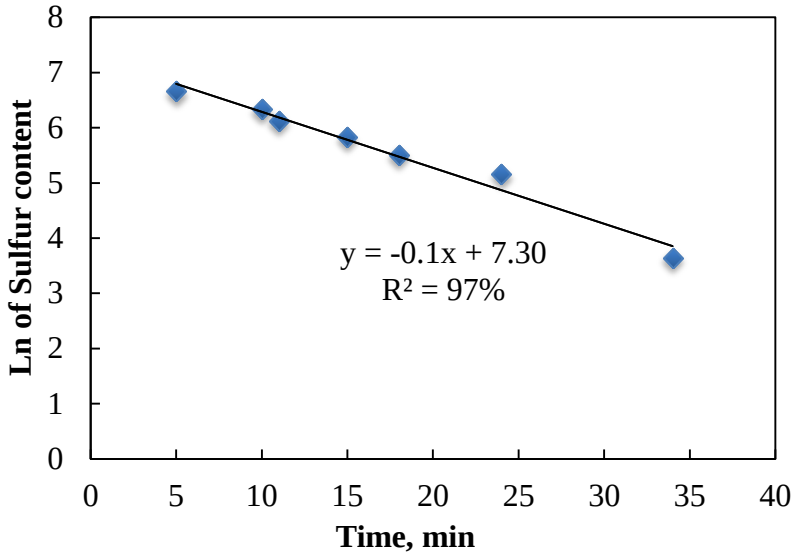

Figure 4.9: Natural logarithm of sulfur concentration over time (same data as Figure 4.8) [115].

Sampling was performed every 15 minutes, at the same time as alumina additions. **Figure 4.10** and **4.11** show the results of experiments with target sulfur levels of 1000 ppm and 500 ppm, respectively. It can be concluded that feeding half of the initially added sulfur amount in 10-minute intervals is sufficient because no underfeeding or overfeeding is seen in **Figure 4.10** and **4.11**.

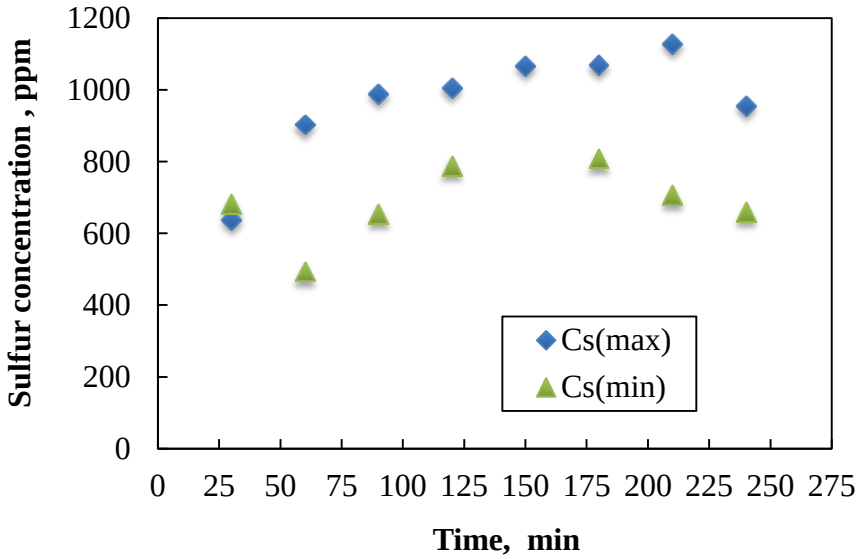

Figure 4.10: Sulfur concentrations in the bath analyzed by ICP (1000 ppm target). c_s(max) are values sampled 5 minutes after sodium sulfate addition; c_s(min) are values sampled 10-minutes post addition.

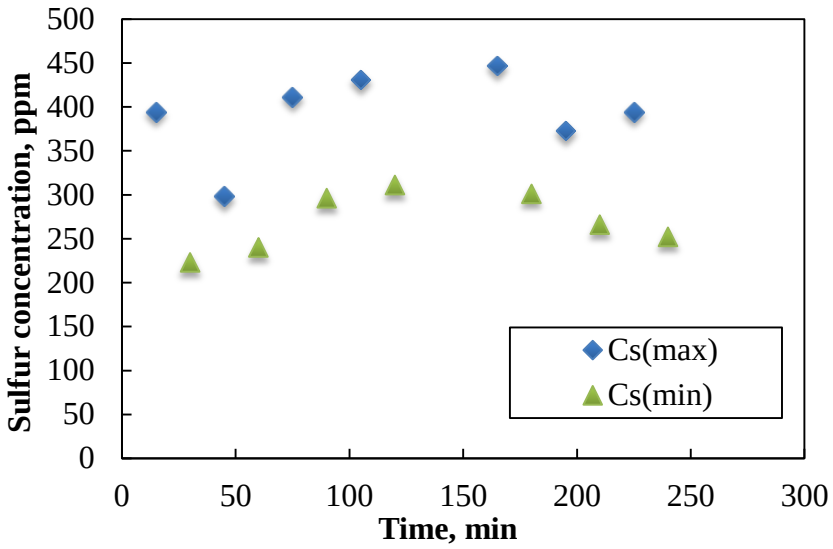

Figure 4.11: Sulfur concentrations in the bath measured by ICP (500 ppm target). c_s(max) are values sampled 5 minutes after sodium sulfate addition; c_s(min) are values sampled 10-minutes post addition.

4.1.3.2 Effect of Sulfur on Current Efficiency *(Supplement 5)*

After establishing the quantity of sodium sulfate required to keep sulfur concentration in the electrolyte constant, the effect of sulfur concentration on CE was studied. CE was reduced by 1.1% for each 100 ppm average sulfur concentration in the bath (**Figure 4.12**). The reported CE loss is based on the average sulfur concentration because sulfur depletes quickly and it is difficult to maintain a constant sulfur concentration in the electrolyte. Therefore, the average concentration of sulfur during electrolysis based on the mean value of the 5- and 10-minute recordings was used. Due to the known detrimental effect of phosphorus, all samples were also analyzed for phosphorus. A significant concentration of phosphorus (50 ppm) was found only in one experiment. Phosphorus concentrations were negligible (0-8 ppm) for all other experiments. The CE was corrected for the outlier experiment by adding 0.5% based on a 1% decrease for each 100 ppm of phosphorus [1-4].

It is likely that the reduction in CE is due to a mechanism similar to phosphorus. Impurities with two or more oxidation states may undergo cyclic red-ox reactions, where the oxidized state reacts with dissolved metal within the diffusion boundary layer at the cathode [116]. At the reaction plane, the concentration of the oxidized state as well as dissolved metal are zero. Higher impurity concentration pushes the reaction plane closer to the cathode, which means that the concentration gradient of the dissolved metal becomes steeper and CE decreases. The reduced form of the impurity formed at the reaction plane is transported back towards the anode, and some part may be further reduced at the cathode.

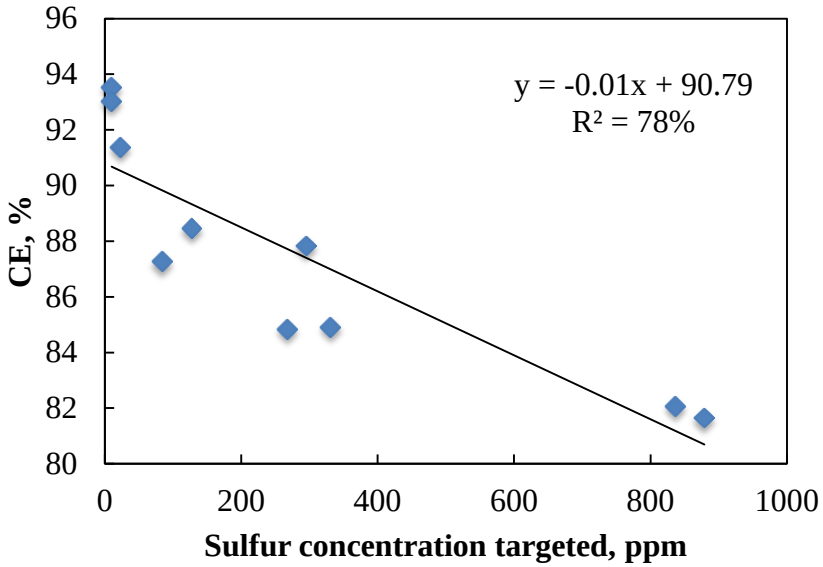

Figure 4.12: CE loss based on the mean value of the 5- and 10-minute recordings at 0.8 A/cm^2 [115].

It is not known whether the reduction in current efficiency is due to the same mechanism as observed for phosphorus. Loss in current efficiency due to the presence of sodium sulfate can be attributed to either a chemical or an electrochemical reaction, or perhaps a combination of the two. In the case of a chemical reaction, the reactants are either carbon [88, 91] or aluminum [67, 91]; possible reactions are found in **Table 2.5**. Both Burnakin et al. [67] and Ambrova et al. [91] reported increased loss of aluminum in the presence of sodium sulfate and carbon. Sulfide can be oxidized electrochemically at the anode according to the following reaction [117]:

$$S^{2-} = S + 2e^{-} \tag{4.3}$$

Probable sequential reactions, which result in the formation of CS_2 and S_2, were proposed by the same authors [117]:

$$S = S_{(ad)} \tag{4.4}$$

followed by

$$S_{(ad)} = S_{2(ad)} \tag{4.5}$$

and/or

$$S_{(ad)} + xC = C_xS_{(ad)} \tag{4.6}$$

$$2C_xS = CS_{2\ (ad)} + (2x-1)C \tag{4.7}$$

It should be noted that gas measurements were performed during the electrolysis, and CS_2 was among the detected gas species (SO_2, COS, CS_2, and H_2S). This is discussed in Section 4.1.3.

Other probable electrochemical reduction reactions (Reaction (2.57) and (2.58)), which occur through 2- or 3-electron transfers, were proposed by Hajasova [73] based on her electrochemical studies of sodium sulfate in cryolite melts.

Another possible explanation for the impact of sulfur on current efficiency is that the addition of sodium sulfate generates large bubbles while being reduced. **Figure 4.13** shows the solidified bath on the bottom of the anode from the 500 ppm target experiment. Several large bubble-like shapes can be seen. Bubble generation can disturb the boundary layer between metal and bath and enhance the rate of the back reaction.

Solidified electrolyte, however, may not be representative of the situation occurring in the liquid electrolyte. Large bubbles cannot survive in the electrolyte. Small bubbles may and may take a long time to be removed. During solidification, small bubbles may grow into larger bubbles as the solubility of gases in the electrolyte decreases upon cooling**.**

Another factor that may have contributed to the loss in CE is the presence of Na ions. Sodium sulfate introduces additional Na ions, which may shift the cryolite ratio (CR = mol NaF/mol AlF_3). Increased sodium fluoride concentration in the bath is reported to decrease CE by 4.3% per unit ratio [113]. This reduction is explained by the enhanced back reaction at the bath-metal interface. Dissolved sodium ions may play a bigger role in metal solubility than aluminum dissolution due to their (sodium ions) electronic properties and the high mobility of associated electrons [17]. XRD analysis of electrolyte samples did not confirm an increase in cryolite ratio; on the contrary, a slight reduction was detected. As a result, the possible cryolite ratio effect was disregarded for the purposes of this study.

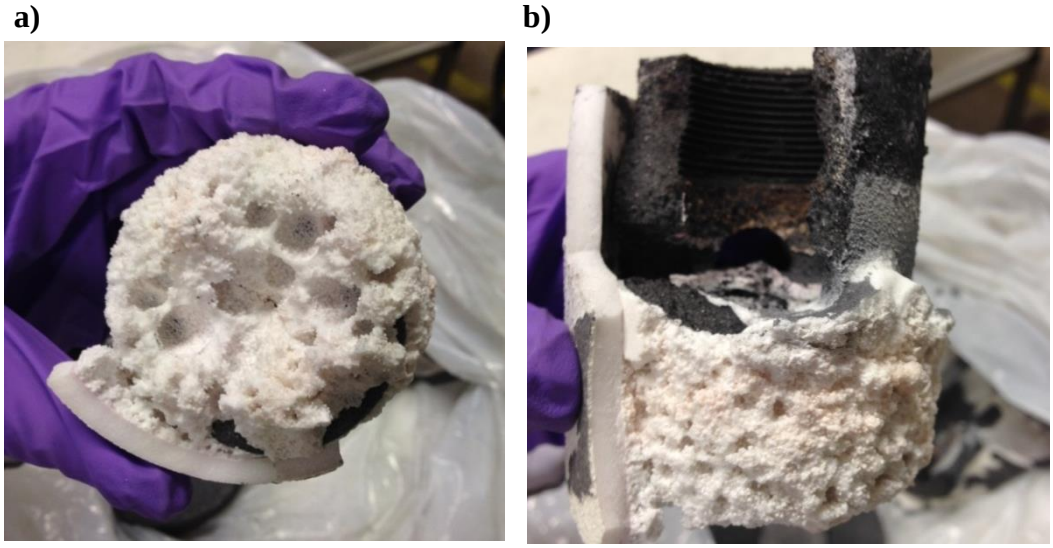

Figure 4.13: Photograph of the solidified bath on the graphite anode: a) view from the bottom of the anode b) view from the side of the anode [115].

4.1.3 Behavior of Sodium Sulfate in Cryolite-Alumina Melts (*Supplement 6*)

Before discussing the results from *Supplement 6*, possible reactions of sulfurous gases and their equilibria will be reviewed. **Table 4.2** lists the possible reactions of sulfurous gases. It clearly shows that COS formation is dependent on Reactions (4.8) and (4.9), which require carbon source.

Anodes are the source of carbon in aluminum electrolysis. Typical source of CO_2 in aluminum electrolysis is the electrochemical reaction at the anode (Reaction 2.1). CO_2 can react with carbon to produce CO by the Boudouard reaction. The back Reaction (2.5) is another source of CO. Oxidation of COS is usually the source of SO_2 in industrial cells. In this laboratory study, COS may be a result of the reduction of sodium sulfate by carbon or aluminum as shown in **Table 2.4**. SO_2 can also be generated by electrochemical reactions as discussed in the Chapter 2. SO_3 is not stable at 980 °C.

In order to understand the behavior of sodium sulfate in aluminum reduction cells and study ongoing reactions and their gaseous products, our experimental test series started with simple systems. Experimental conditions were gradually switched to those found in industrial cells. A full industrial test (T5) is discussed in Chapter 4.2.

Table 4.2: Sulfurous gas reactions in aluminum electrolysis cells [118]. Gibbs energies are calculated by the HSC 7.1 software and given in kJ/mol.

Reaction	$\Delta_r G°$ at 100 °C	$\Delta_r G°$ at 980 °C	
$SO_2 + 3CO = COS + 2CO_2$	-232.6	-72.2	(4.8)
$SO_2 + 2C = COS + CO$	-19.1	-170.9	(4.9)
$COS+½C = ½CS_2 + CO$	59.1	-13.5	(4.10)
$COS + H_2O = H_2S + CO_2$	-29.8	-27.5	(4.11)
$SO_3 = SO_2 + ½O_2$	63.84	-18.7	(4.12)
$SO_3 + 2C = COS + CO_2$	-205.9	-362.9	(4.13)

A brief summary of the details and results of all our tests is given in **Table 4.3**. Bath samples were analyzed by ICP spectroscopy and ion chromatography. Ion chromatography was used to investigate whether sulfide was formed under different conditions. The results of this test were inconclusive. Furnace off-gases were passed through a mass spectrometer for qualitative assessment. Mass spectrometry allowed us to understand the type of gas products formed during the reactions.

The purpose of the T1 experiment was to investigate which gaseous compounds formed when reducing agents (C, Al) were introduced. The effect of the reducing agents on sodium sulfate stability was studied at the same time. For this test, the molten electrolyte was kept inside a corundum crucible. The T1 test consisted of: melt without reducing agents (T1a), melt with graphite (T1b), and melt with graphite

and aluminum (T1c). Pieces of graphite with an approximate total surface area equal to 12 cm^2 served as the carbon source. The total weight of aluminum was 12.9 grams.

Experiment T2 had similar conditions as T1. However, reducing agents were introduced into the current efficiency cell (shown in Chapter 3) .The experiment also included a test phase including electrolysis. Sulfur stability and formed gas species were compared under different conditions. T2 consisted of: melt with carbon (T2a), melt during electrolysis (T2b), and melt with carbon and aluminum (T2c). The graphite anode was lowered by 2 cm into the melt before the start of the experiment giving a total surface area of 35.5 cm^2.

Experiments T3 and T4 studied the effect of sulfur on current efficiency with half of the target level of sulfur added every 10 minutes.

Electrolyte sample analysis by ICP for tests T1 and T2 is shown in **Figure 4.14**. Sodium sulfate appears quite stable in alumina-cryolite melts with total sulfur half-life equal to 231 minutes (T1a). When carbon (graphite) was added into the system, the half-life was reduced to 116 minutes (T1b). In the presence of both carbon and aluminum, the half-life was only 29 minutes (T1c).

In experiment T2a, the half-life of sodium sulfate in the presence of carbon was 39 minutes, much shorter than the 116 minutes seen in experiment T1b. The reason is most likely the larger surface area of carbon available for the reaction in experiment T2a (35.53 cm^2 versus 12 cm^2).

Table 4.3: Summary of the tests [118]. "S target" is the sulfur target added into the melt, "S melt" is the sulfur content at the beginning of the experiment determined by ICP-MS, "C" is carbon, "Al" is aluminum, "El" is electrolysis, and "nA" is detector current response given in nanoampere.

Test	Time	C	Al	El	S target	S melt	Av. CO_2	Av. COS	Av. SO_2	Av. CS_2	Av. H_2S	t1/2
	min				ppm	ppm	nA	nA	nA	nA	nA	min
T1a	0-120	-	-	-	1000	855	5	0.06	0.32	0.18	0.09	231
T1b	120-180	+	-	-	-	624	21	0.15	0.91	0.46	0.12	116
T1c	180-240	+	+	-	-	452	12	0.16	0.33	0.50	0.17	29
T2a	0-120	+	-	-	1000	909	36	0.16	0.07	0.36	0.25	39
T2b	120-180	+	+	+	-	136	1393	1.03	0.35	0.46	0.28	8
T2c	180-300	+	+	-	1000	1086	425	0.73	0.80	0.39	0.25	28
T3	0-240	+	+	+	1000	836	686	3.28	15.95	0.72	0.92	-
T4	0-240	+	+	+	500	573	372	1.71	2.51	0.11	0.66	-
T5	0-60	+	+	+	1000	776	-	-	-	-	-	5

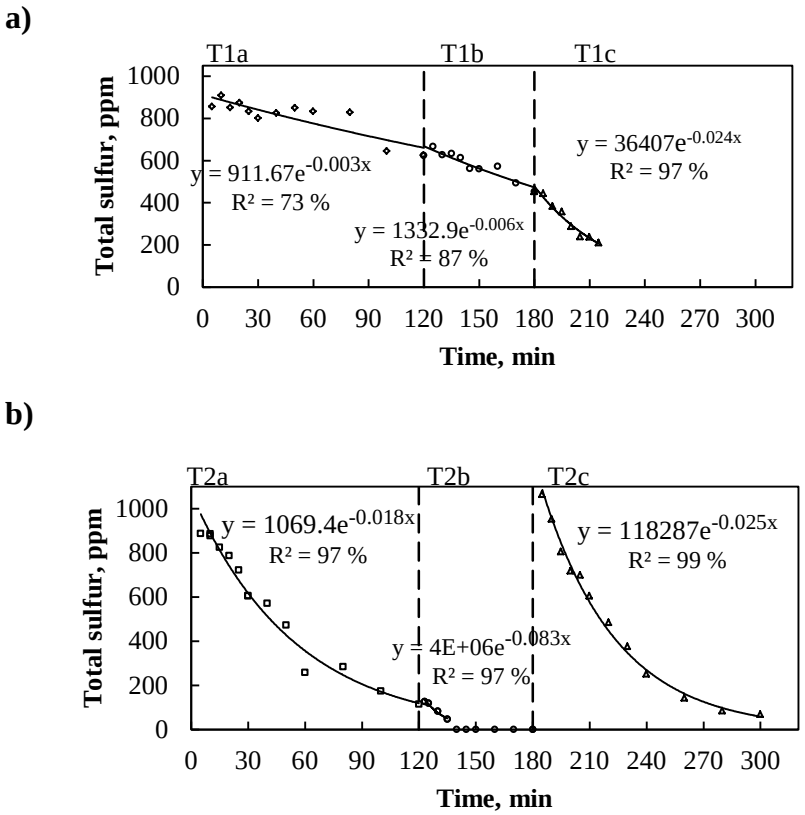

Figure 4.14: **a)** Total sulfur concentration as a function of time for the test series T1a, T1b, and T1c; **b)** Total sulfur concentration as a function of time for the test series T2a, T2b, and T2c. Vertical dashed lines indicate the start of new test condition [118].

Test T2 explores sulfur stability during electrolysis. One of the decay curves of sulfur concentration over time was given earlier in **Figure 4.8**. Remaining sulfur concentration in the electrolyte was low (136 ppm) when the test was started (compared to other tests, which contained 450-800 ppm of sulfur). Nevertheless, the half-life of sulfur content was found to be 8 minutes, a value in agreement with a prior test beginning at 776 ppm sulfur (**Figure 4.8** also shows 7 minutes).

The T2c condition showed a similar half-life (28 minutes) as T1c (29 minutes) despite T2c having a larger surface area of carbon in the electrolyte.

Electrolyte analysis of T3 and T4 was presented in section 4.1.3.1 (**Figure 4.10** and **Figure 4.11**). T3 was conducted with a target sulfur level of 1000 ppm. Half of the initial target was added every 10 minutes to compensate for sulfur loss (Figure 4.10). The same procedure was done during T4, but a lower target sulfur level was set (500 ppm).

Gas measurements from test T1a showed very limited release of gases when no reducing agents were present (**Figure 4.15**). The presence of signals for COS when no carbon was present in the electrolyte can be explained by gas reactions with the graphite support holding the alumina crucible.

A four-fold increase in CO_2 signal intensity was observed after carbon addition. The signals for SO_2 and CS_2 increased by 2.8 and 2.5 times, respectively. The intensity of H_2S was largely unaffected. CS_2 emissions have not been well understood or explained in the literature. It is of interest then that CS_2 is observed when sulfur is present in the melt along with a piece of carbon. Possible routes for CS_2 formation are Reactions (4.14) and (4.15) with standard Gibbs free energies of -989 kJ and -89 kJ, respectively, at 980 °C:

$$3Na_2SO_4 + 21/2C + 2AlF_3 = 3/2CS_2 + Al_2O_3 + 6NaF + 9CO \quad (4.14)$$

$$2Na_2SO_4 + 7C = CS_2 + 2Na_2O + 6CO \quad (4.15)$$

After the addition of aluminum into the crucible (T1c), the signals for all sulfurous gases increased significantly (**Figure 4.15**). Shortly after the initial increase, the gas signals ceased completely.

T2a has a slightly higher CO_2 signal intensity than T1b despite similar test conditions (**Figure 4.16**). COS and CS_2 intensities are similar, but SO_2 is 13 times lower. H_2S is doubled, which can be expected as a new addition was made in T2a.

The T2b condition explores sulfur stability under electrolyzing conditions. Even though the remaining sulfur concentration in the electrolyte was low, the COS signal intensity of T2b is 4.4 times higher than that observed in experiment T1. This suggests that sodium sulfate is very reactive and quickly depleted under electrolyzing conditions. This hypothesis is supported by electrolyte sample analysis and gas measurements.

During test T2c (same conditions as T1c), the intensity of H_2S and CS_2 sulfurous gases was of the same order of magnitude as during test T1c. However, COS and SO_2 signal intensities were much higher. Since electrolysis was run during the earlier experiment, the electrolyte may have contained enough dissolved CO_2 to allow for COS formation (see **Figure 16**). T3 and T4 were conducted with half the amount of sulfur: 500 ppm out of an initial concentration (1000 ppm) was added every ten minutes to compensate for sulfur loss (**Figure 4.10** and **4.11**). Gas analysis for T3 and T4 during electrolysis is presented in tabulated format in **Table 4.3**. A graphic illustration is given only for T3 in **Figure 4.17**. An interesting observation was made when electrolysis was stopped after 240 minutes, but sulfur additions continued to be made every 10 minutes in **Figure 4.17**. It shows that most of the sulfurous gases continued to be formed with the exception of COS. COS decreased along with the CO_2 signal. A similar effect was observed in experiment T3.

A comparison of gas analysis data from experiments T1b/T1c (no electrolysis, but C and Al were present) and T2b (electrolysis) reveals striking similarities. CO_2, SO_2, COS, and CS_2 are present in the gas phase in all experiments. This shows that sodium sulfate gets decomposed simply by the presence of carbon or aluminum. It implies that sodium sulfate is not stable in this environment. However, analysis of bath samples from industrial aluminum cells detected the presence of both sulfate and

sulfide [119]. It probably means that sulfate can be present in the anode region where oxidizing conditions prevail, while sulfide is stable in the cathode region. Red-ox reactions may take place [117].

Compiling all the gas analysis results reveals that the concentration of COS is generally higher when CO_2 concentration is higher (**Table 4.3**). This underlines the importance of CO_2 in COS formation. It suggests that COS is formed after CO_2 is first produced. The T2b electrolysis test identified COS as the main sulfur-containing gas, which is in agreement with literature [81, 82]. The tests with continuous addition of sodium sulfate, on the other hand, favor SO_2 as the main sulfurous gas.

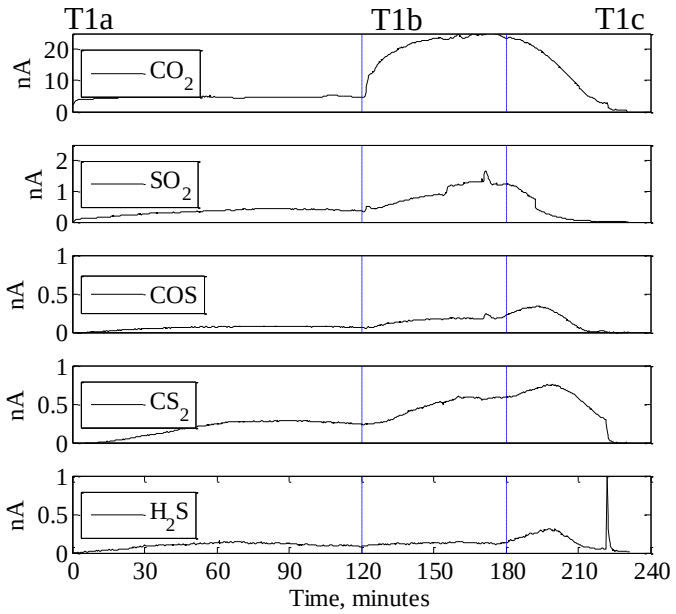

Figure 4.15: Gas analysis of experiment T1. Gas species are divided into separate subplots to avoid overlap between signals. Vertical lines indicate the start of new test conditions: (T1a (0-120 minutes), T1b (120-180 minutes), and T1c (180-240 minutes).

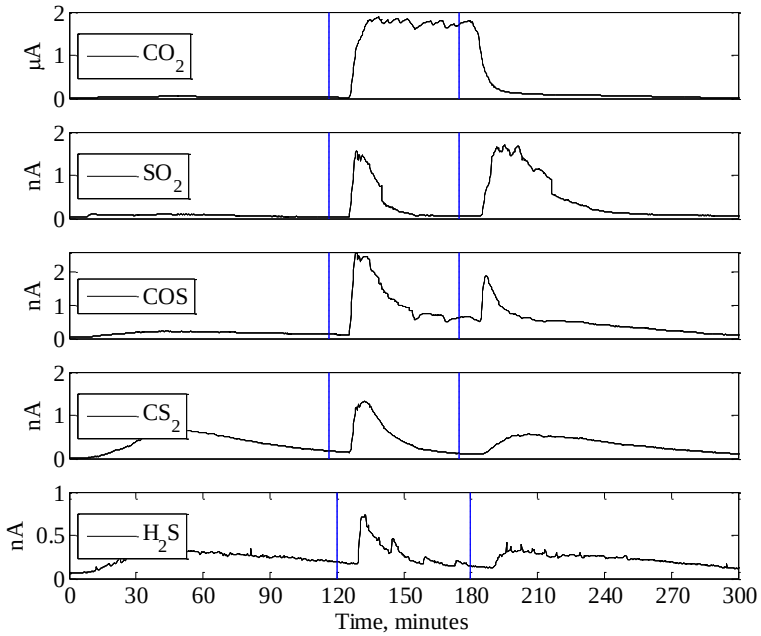

Figure 4.16: Gas analysis for experiment T2. Gas species are divided into separate subplots to avoid overlap between signals. Vertical lines indicate the start of new test conditions: (T2a (0-120 minutes), T2b (120-180 minutes), and T2c (180-300 minutes).

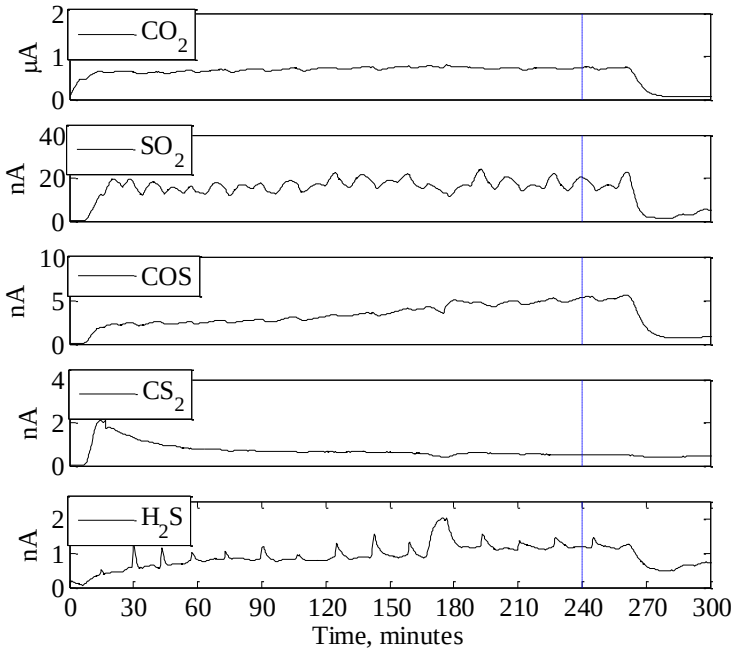

Figure 4.17: Gas analysis for experiment T3. Electrolysis was run with a target sulfur level of 1000 ppm. To compensate for sulfur loss during electrolysis, half of the amount of sulfur initially added was added to the electrolyte in 10-minute intervals. Vertical lines indicate the end of electrolysis.

4.2. Industrial Studies

4.2.1. Plant Data Analysis (*Supplement 4*)

Industrial plant data covering the period from January 2011 to December 2013 were examined. Cell-to-cell variability of phosphorus was found to be a function of a number of different process parameters. The effect of these parameters on phosphorus concentration in the metal is summarized in **Figures 4.18 - 4.21** (from S*upplement 4*). Higher bath height was correlated with higher phosphorus concentration in the metal (see **Figure 4.18**). This is probably a result of higher probability of anode effects at lower bath heights. Anode effects increase convection and induce faster evaporation of phosphorus. Haugland et al. [30] reported that anode effects reduce phosphorus concentration in the metal. However, nowadays anode effects are killed so quickly that electrolyte overheating should be limited. On the other hand, anode effects can increase anode and bath surface temperatures, where most carbon dust is located. Due to strict regulations of emissions, experiments with phosphorus and anode effects could not be performed at the plant. However, one incident was observed where phosphorus in the electrolyte and the metal dropped by 57% and 25%, respectively, after an anode effect occurred. Another explanation for the strong correlation between high electrolyte levels and high phosphorus could be the contamination of electrolyte by cast iron that surrounds the steel stubs. Cast iron that fills the voids between anodes and steel stubs can contain phosphorus (0.06-0.22 wt% for the particular cells investigated).

Haugland et al. [30] observed a correlation between phosphorus and electrolyte temperature. They found that phosphorus concentration decreased with increasing temperature. In this study, the relationship between phosphorus and temperature does not support a statistically significant correlation. According to **Figure 4.19**, low levels of phosphorus are present at high temperature. The effect of temperature levels off at higher phosphorus levels.

Phosphorus in the metal was strongly correlated with superheat (**Figure 4.20**). Side ledge melts and baths are diluted at higher superheat. Additionally, higher bath temperature facilitate evaporation of phosphorus-containing species. At lower superheat, a larger fraction of the bath is frozen as a ledge. Phosphorus and other impurities have a relatively small volume of liquid bath to dissolve in, resulting in high concentrations of phosphorus in the electrolyte and consequently in the metal.

Close monitoring of raw material quality is paramount. Once phosphorous is in the system, it will continue to circulate and is hard to remove. **Figure 4.21** shows a 0.69 ppm increase in phosphorus in the metal per year. This contradicts the statistical analysis of Danek et al. [31], who concluded that P_2O_5 concentration in the electrolyte decreases over time. However, the statistical analysis was performed within a one-year period. It might therefore not be directly comparable to the present study. Colder temperature of older cells may be behind the correlation of cell age and phosphorus concentration. Old cells serve as a sink for phosphorus because all the evaporated phosphorus is forced back to the cells through secondary alumina. Therefore,

phosphorus may accumulate in some cold cells as only a small portion will be able to escape through dry scrubbers and the metal. Higher phosphorus levels is the cast iron used for cathode castings may likewise be a contributor. A thinning cathode over time could reduce the diffusion length required for phosphorus to make it to the metal.

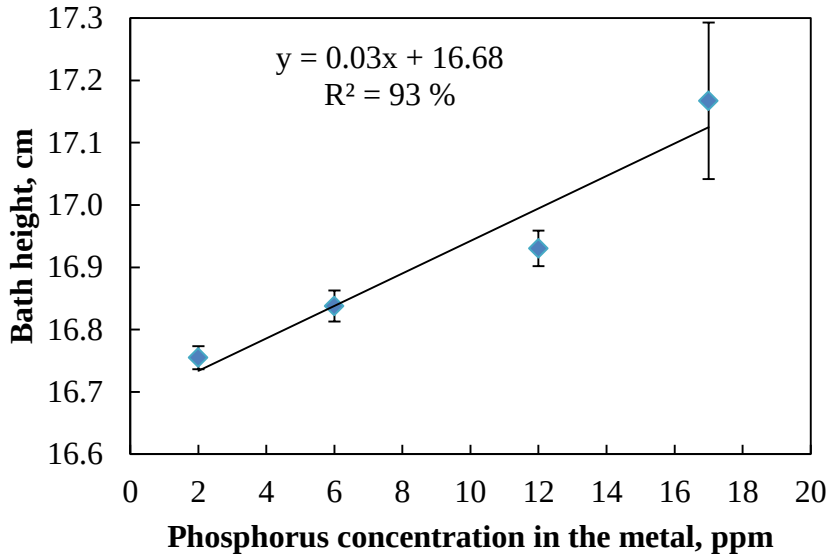

Figure 4.18: Bath height versus phosphorus concentration in the metal (January 2011-December 2014). Error bars were constructed using standard error of the mean [106].

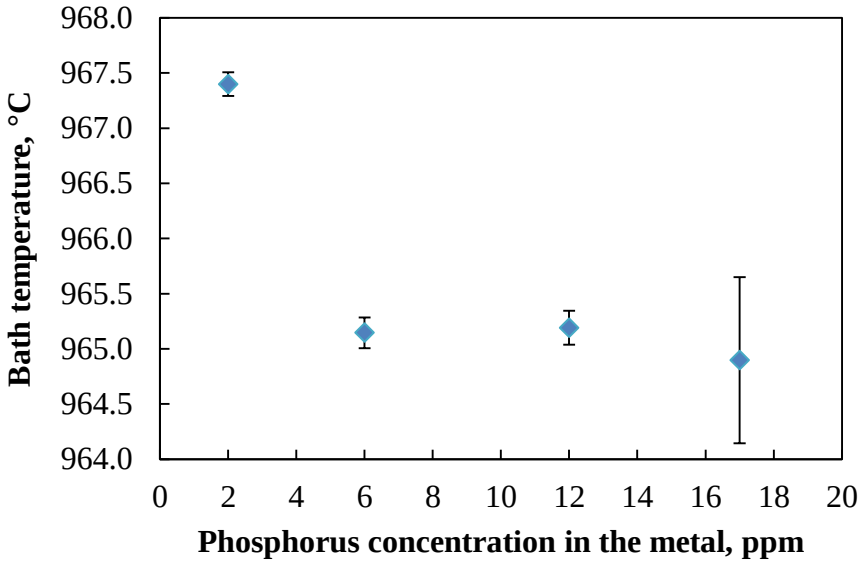

Figure 4.19: Bath temperature versus phosphorus concentration in the metal (January 2011-December 2014). Error bars were constructed using standard error of the mean [106].

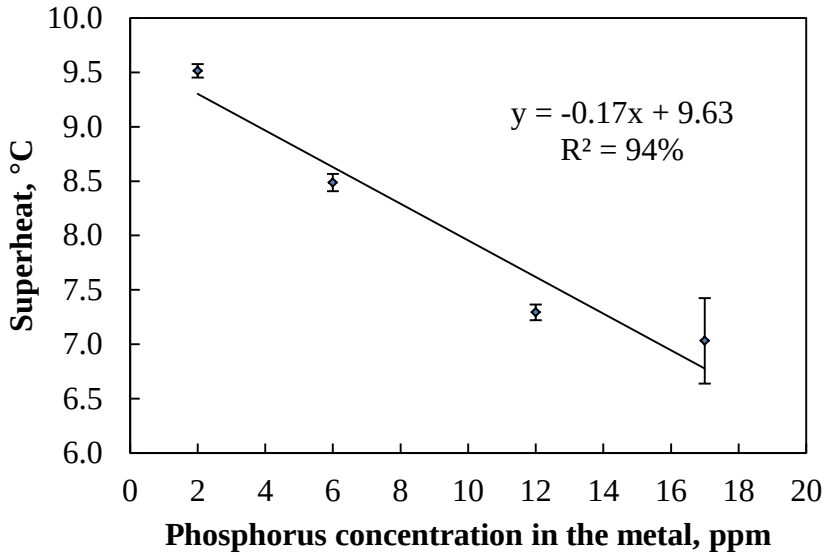

Figure 4.20: Superheat versus phosphorus concentration in the metal (January 2011-December 2013) [106].

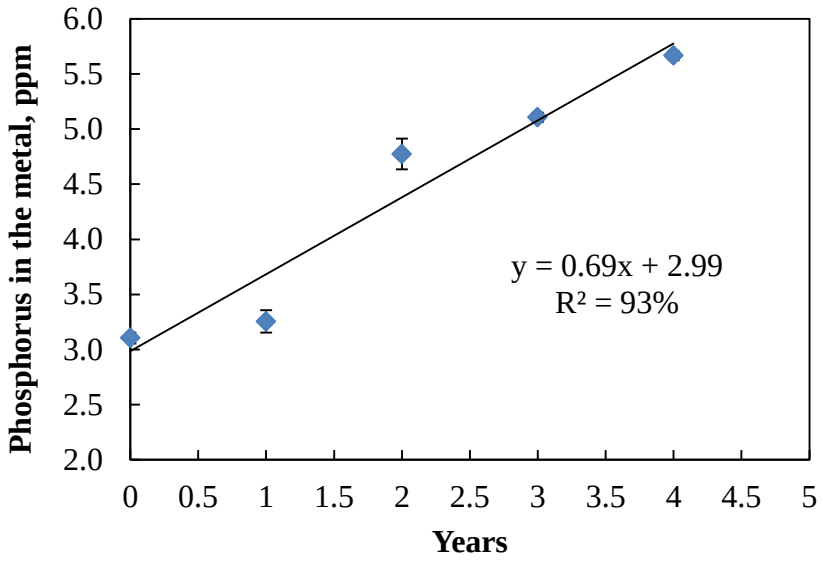

Figure 4.21 Evolution of phosphorus concentration in the metal over 5 years after startup (January 2011-December 2013) [106].

4.2.2 Behavior of Impurities during Current Interruption (*Supplement 4*)

Power outages were utilized to further explore the behavior of impurities under different conditions. Power outages provide an opportunity to discover if electrolysis

has an effect on the distribution of impurities. All tests were repeated twice. Three cells were tested during the first trial, and the results were contradictory. In order to collect more reliable results, tests were repeated using a new sampling device as discussed in Chapter 3. The test was performed on one cell, but bath samples were collected from three electrolyte heights (surface, middle, and at the metal pad).

Each power outage lasted one and a half hours. Temperature of the cell decreased by 34 °C, and electrolyte level dropped from 17 cm to 15 cm.

The results confirmed that power outages do affect impurity distribution. The concentration of both phosphorus and sulfur increased when current was interrupted (**Figure 4.22** and **4.23)**. Data points towards the end of the power outage are missing because removal of electrolyte samples (especially from the middle of the electrolyte and close to the metal pad) became impossible due to the mixing of electrolyte with the aluminum. However, there was no problem with metal sampling. Phosphorus concentration in the metal (see *Supplement 4*) increased during the power outage, which supports the results in **Figure 4.22**. Increases in impurities during a power outage may be due to reduced convection, which lowers the ability of the phosphorus and sulfur species to escape to the gas phase either as gaseous species or via carbon dust particles. Another hypothesis is that phosphorus and sulfur originate from anodes or carbon dust. When current is cut, the anode is no longer positively charged. The anode releases phosphorus anions accumulated during electrolysis back into the cell. Thisted [1] performed both industrial and laboratory studies and observed a decrease in phosphorus concentration during current interruption. Jentoftsen [117] focused on the behavior of iron during current interruption. He reported a decrease in iron concentration in the electrolyte from the same test campaign conducted with Thisted [1]. Thisted [1] commented that other impurities (Si, Ti, and Mn) were also added together with phosphorus and iron, but they were more or less unaffected by the power outage. The authors explained that the decrease in impurities during current interruption may be due to the transfer of phosphorus via carbon particles towards the electrolyte surface. Dissolved aluminum in the electrolyte increases and can also react with metallic impurities. Solidification of some impurities in the side ledge was also suggested. Both authors observed higher concentrations of the elements in the metal phase. Keep in mind that both studies added impurities artificially, whereas in this study impurities were not added into the electrolyte.

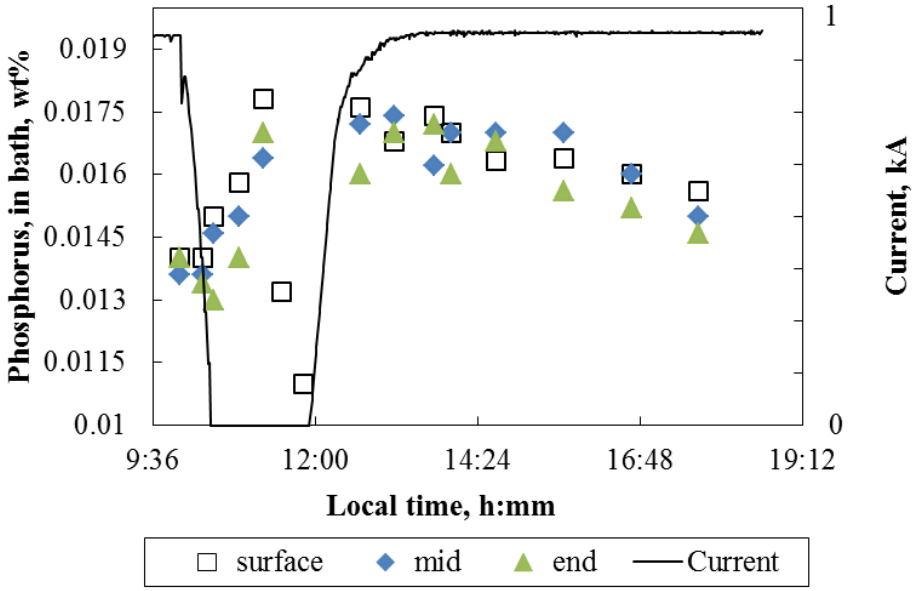

Figure 4.22: Concentration of phosphorus in the bath and line current as a function of time [106].

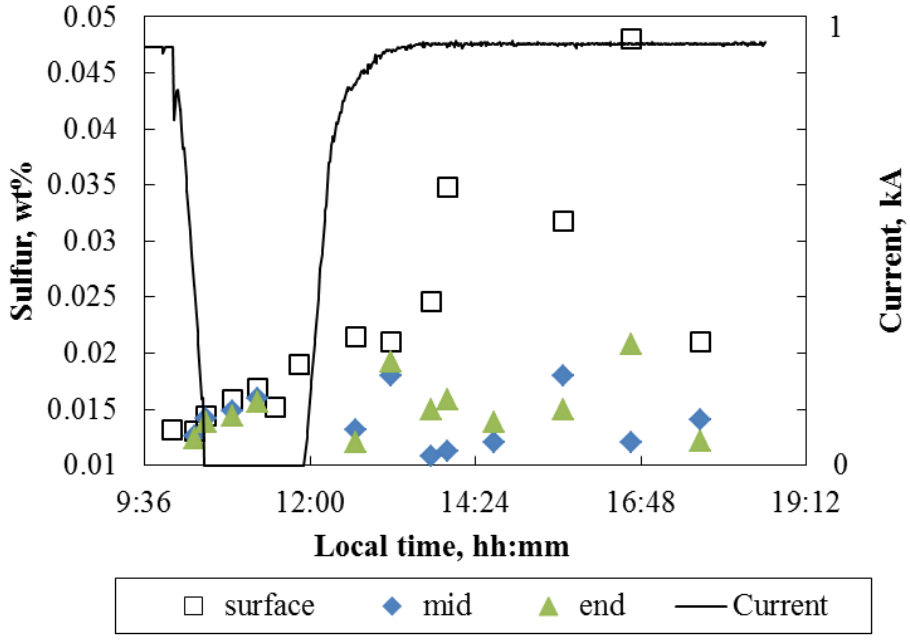

Figure 4.23: Concentration of sulfur in the bath and line current as a function of time [106].

4.2.3. Sodium Sulfate Addition Tests (*Supplement 6*)

Sodium sulfate was added to an industrial electrolysis cell through the tapping hole and the alumina feeder holes. A target of 1000 ppm of sulfur in the electrolyte

was set (as described in Chapter 3.3.1). Measurements of sulfur in the electrolyte were obtained with the aim of evaluating sulfur loss from the electrolyte over time (**Figure 4.24**). The purpose of this experiment was to ensure that the level of sulfur in the bath is well-controlled during the experiments designed to measure the effect of sulfate addition on current efficiency. The half-life of sulfur in the electrolyte was similar to that observed in laboratory tests (5 minutes). As sulfur depletes very fast, frequent additions would have been required to maintain a constant electrolyte sulfur concentration. The experiment was abandoned due to environmental restrictions. Cell resistance increased significantly during these tests. **Figure 4.25** shows the increase in cell resistance during sodium sulfate addition. Repeated tests confirmed the effect of sodium sulfate on cell resistance. According to **Figure 4.25**, 800 ppm of sulfur in the electrolyte causes an approximately 370 mV increase in voltage. This represents about a 10% increase in energy consumption over this short period.

To the best of our knowledge, the effect of sodium sulfate addition on cell resistance has never been reported in literature. Burnakin et al. [83] determined the resistivity of baked anode mass and found that an increase in anode sulfur content by 1% leads to an increase in anode ohmic resistivity by 12%. It was commented that this rise could cause an increase in specific energy consumption.

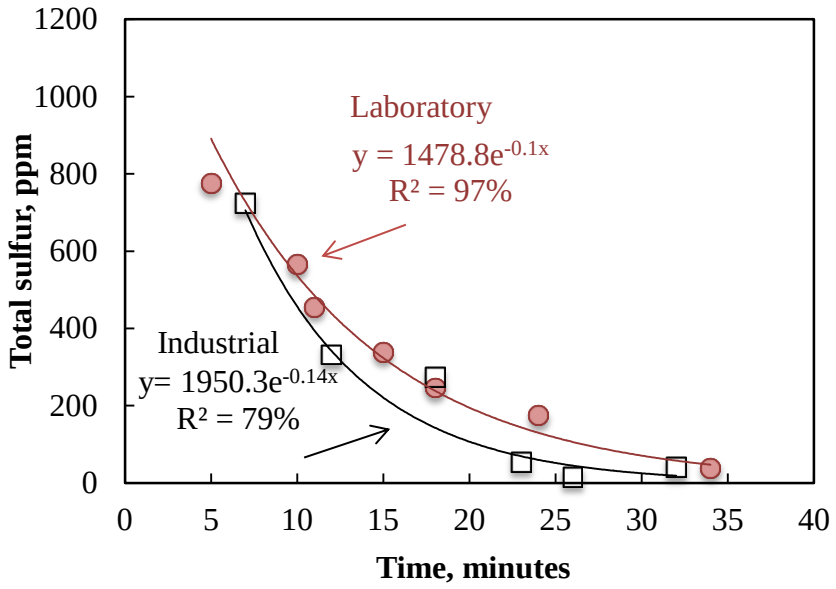

Figure 4.24: Comparison of sulfur decay curves between the laboratory electrolysis test and industrial electrolysis test (T5) after addition of 0.44 wt% of sodium sulfate (1000 ppm sulfur). Electrolyte samples from the laboratory and industrial test were analyzed by ICP and X-Ray Fluorescence, respectively.

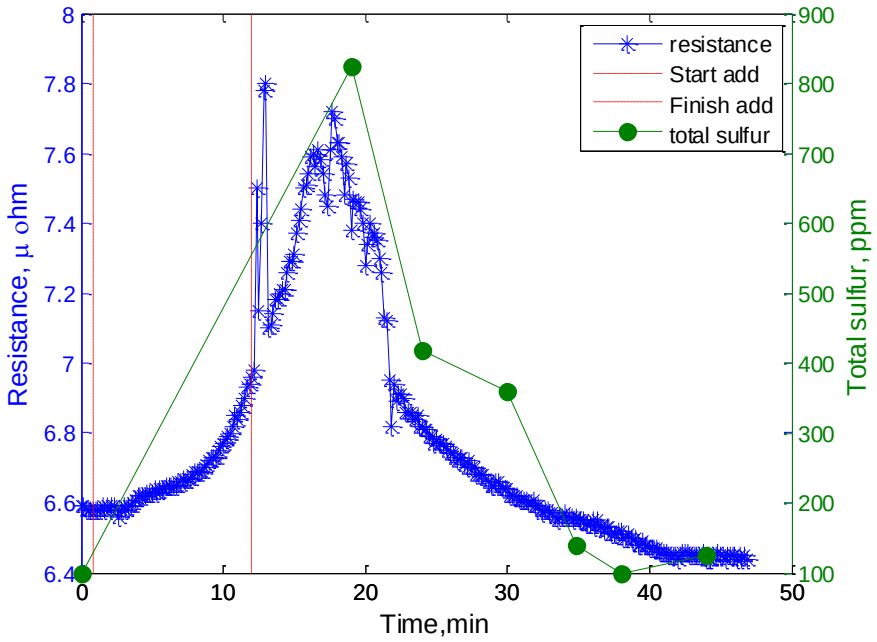

Figure 4.25: Cell resistance and sulfur concentration during sodium sulfate (0.44 wt%) addition to an industrial cell [118].

5 FUTURE WORK AND CONCLUSION

5.1 Future Work

Results concerning the negative effect of sulfur on current efficiency should be confirmed by running experiments with anodes of varying sulfur content. This effect has already been demonstrated in laboratory tests [11], but it needs to be verified at full scale tests in industrial cells.

Effect of sulfur on current efficiency at higher current densities was not tested, but understanding the behavior of sulfur in aluminum electrolysis at higher current density is of interest. Based on the higher impact of phosphorus at high current densities, it is likely that interest in impurities will grow within the industry as current densities in commercial cells increase.

Supplementary studies to improve the understanding of the behavior of impurities in industrial cells revealed interesting results that could be expanded on. Correlations found between phosphorus and different operational parameters from statistical analysis would benefit from experimental verification.

The positive effect of current density on current efficiency was found to have a maximum for the particular cell design used. It would be worthwhile to study the mechanisms and take these into account when developing new cell designs with different flow patterns and anode designs to facilitate further current efficiency increases. As industry is likely to continue to raise current density to increase productivity, the demand for a new cell design to conduct experiments at higher current densities will increase.

The effect of sulfur on cell resistivity found during sodium sulfate additions into industrial cells is certainly worth investigating further as the increase in resistivity was found to be significant and confirmed by two industrial tests.

5.2. Conclusions

We studied the influence of current density on current efficiency in a laboratory cell and showed that increasing cathodic current density above 1.5 A/cm^2 lowers current efficiency. This may due to enhanced gas evolution and stirring in the cell, or more complex fluid flow phenomena like magneto hydro dynamics (MHD) may be at play. Increased stirring of the electrolyte can reduce diffusion layer thickness and enhance transport phenomena, which will in turn increase the rate of the back

reaction. The specific behavior of current efficiency as a function of current density is dependent on the cell set-up and bath composition (cryolite ratio, presence of additives). The observed reduction of current efficiency above 1.5 A/cm^2 might not apply to other cell designs with different flow patterns and conditions.

Electrolyte samples taken during electrolysis and analyzed by ICP showed that, after the initial addition of phosphate, phosphorus levels drop by only a small amount from the initial level at the beginning of the experiment and stays constant throughout the entire experiment. Additions to compensate for the loss during electrolysis are thus unnecessary. We developed a technique to determine the average phosphorus concentration in the bath depending on the added amount of phosphorus. The technique was employed to correct data from earlier studies.

The control study performed at 0.8 A/cm^2 to investigate the effect of phosphorus on current efficiency found that, on average, phosphorus reduces current efficiency by 0.67% per 100 ppm average phosphorus in the electrolyte over the whole range of phosphorus levels studied (0 to 630 ppm). This is in agreement with previous findings by Solli [2] and Thisted [3]. At a higher current density of 1.5 A/cm^2, phosphorus was found to exert an even greater effect with a current efficiency reduction of 1.1% per 100 ppm. The difference is more pronounced if regression analysis is performed for concentrations of industrial interest (0-230 ppm). A reduction of 2.41% per 100 ppm of phosphorus is predicted at 1.5 A/cm^2 compared to 0.92% per 100 ppm of phosphorus at 0.8 A/cm^2 for the same range of concentration**.**

Analysis of industrial data suggests that phosphorus variability between pots depends on a number of operational process parameters. Lower superheat and higher electrolyte height were found to strongly correlate with higher phosphorus concentration in the metal. The correlation of high phosphorus with high electrolyte levels is possibly due to a lower occurrence of anode effects (these increase temperature and convection). It is also possible that higher levels of electrolyte can reach the cast iron, which surrounds the steel stubs and contains some phosphorus. The observed relationship between superheat and phosphorus can be due to a temperature effect or to the fact that higher superheat causes an increase in electrolyte volume. Volumentric concentration of phosphorus will therefore decrease. Phosphorus concentration in the metal is also shown to increase with cell age. This cannot be attributed purely to long residence time of phosphorus in the electrolyte proven by laboratory tests. Older cells are colder and material deterioration can cause an increase in phosphorus concentration. This highlights the importance of controlling phosphorus levels in all raw materials both in direct and indirect contact with the electrolyte or metal.

Current interruptions were found to have an effect on the distribution of impurities. Increases in phosphorus and sulfur concentrations in the electrolyte were observed during power outages.

A suitable sampling device for electrolyte sampling was found to be a crucial tool for the study of impurities, especially in industrial cells. The surface of the electrolyte can contain carbon dust, which is difficult to separate using the common sampling device (iron spatula). Carbon dust is reported to serve as a nucleation site for

impurities such as phosphorus [14]. Chemical analysis showed that sulfur in the electrolyte increases with carbon dust, further supporting these claims. A new sampling device adapted from Rolseth [108] showed good reproducibility between samples, particularly for sulfur (94.8 ± 11.0 ppm). The iron spatula produced large standard deviation in samples from same cell (461.4 ± 370.2 ppm). Phosphorus concentration seemed unaffected by the sampling method.

A methodology using sodium sulfate to maintain a constant concentration of sulfur during electrolysis was designed. Sodium sulfate was found to be very reactive and deplete rapidly in the electrolyte of aluminum reduction cell. Sodium sulfate was added every 10 minutes based on the half-life of sulfur in the electrolyte found from the exponential decay curve. The reported sulfur effect on current efficiency is based on average sulfur concentration in the electrolyte. Detrimental effect of sulfur was confirmed: current efficiency was reduced by 1.1% for each 100 ppm average sulfur concentration in the electrolyte.

In order to find out which effect was contributing the most for the rapid decay of sulfur in aluminum reduction cells, sodium sulfate was tested by slowly introducing known reducing agents (carbon and aluminum). The effect of electrolysis on sulfur stability in the melt was tested in separate test aswell. Off-gases were analyzed by MS spectroscopy to elucidate which reactions were taking place at different conditions. It was confirmed that sodium sulfate is reduced by carbon and aluminum. The half-life was found to be 231 minutes without reducing agents, 116 minutes in the presence of carbon, 29 minutes in the presence of both aluminum and carbon, and 5-8 minutes during electrolysis.

The gas analysis results indicated that CS_2 is formed whenever there is a source of sulfur and carbon in the electrolyte. COS level was also found to follow the CO_2 and cease when no CO_2 was present.

6 REFERENCES

[1] E.W. Thisted, "Electrochemical Properties of Phosphorus Compounds in Fluoride Melts cells", Ph.D. dissertation, Norwegian University of Science and Technology, Trondheim, Norway 2003.

[2] P.A. Solli, "Current Efficiency in Aluminium Electrolysis cells", Ph.D. dissertation, Norwegian University of Science and Technology, Trondheim, Norway 1993

[3] Å. Sterten, P. A. Solli, & E. Skybakmoen, "Influence of Electrolyte Impurities on Current Efficiency in Aluminium Electrolysis Cells", J. of Applied Electrochem., 28(8), pp.781-789, 1998.

[4] L. Deininger and J. Gerlach, "Stromausbeutemessungen bei der Aluminiumoxidreduktionselektrolyse in Laboratoriumszellen, Metall", 33, 131, 1979.

[5] L. Edwards, "The History and Future Challenges of Calcined Petroleum Coke Production and Use in Aluminum Smelting", JOM, pp.1-14., 2014.

[6] M. Sørlie, Z. Kuang, and J. Thonstad, "Effect of Sulphur on Anode Reactivity and Electrolytic Consumption", in Light Metals 2014, pp. 659-665.

[7] H. Kuang, J. Thonstad and M. Sørlie, "Effects of Additives on the Electrolytic Consumption of Carbon Anodes in Aluminium Electrolysis", Carbon,. 33 (10), 1995.

[8] T. Eidet, M. Sørlie and J. Thonstad, "Effects of Iron and Sulphur on the air and CO_2 reactivity of the cokes", Light Metals 1997, pp. 511-517.

[9] R. A. Cahill, R. E. Gehlbach, and G. S. Tittle, "Factors Influencing the Carboxy Reactivity of Calcined Coke". Light Metals 2000, 563-568.

[10] G. P. Gilmore and V. L. Bullough, "A Study on the Effects of Anode Coke Sulfur Content on the Operation of Side Pin Soderberg cells", Light Metals 1982, pp. 741-752.

[11] S. Pietrzyk and J. Thonstad, "Influence of the Sulphur Content in the Carbon Anodes in Aluminium Electrolysis- a Laboratory Study", Light Metals 2012, pp.659-664

[12] K. Grjotheim, C. Krohn, M. Malinovsky, K. Matiasovsky, J. Thonstad, Aluminium Electrolysis – Fundamentals of the Hall-Héroult Process, 2nd ed., Aluminium-Verlag GmbH, Düsseldorf, Germany, 1982.

[13] K. Grjotheim and H. Kvande, "Introduction to Aluminium Electrolysis", Aluminium-Verlag GmbH, Düsseldorf, Germany, 1993.

[14] J. Thonstad, P. Fellner, G.M. Haarberg, J. Híveš, H. Kvande, and Å. Sterten Aluminum Electrolysis – Fundamentals of the Hall-Héroult process, 3rd ed., (Aluminium-Verlag GmbH, Düsseldorf, Germany, 2001).

[15] A. Pedchenko, S. Molokov, J. Priede, A. Lukyanov and P. J. Thomas, “Experimental Model of the Interfacial Instability in Aluminium Reduction Cells”, EPL (Europhysics Letters), 88(2), 24001, 2009.

[16] H. A. Øye, “Long Life for High Amperage Cells”, Scandinavian Journal of metallurgy, 30(6), pp. 415-419,2001

[17] A. Solheim, Current Efficiency in Aluminum Reduction Cells: Theories, Models, Concepts, and Speculations, Light Metals 2014, pp. 753-758

[18] A. T. Tabereaux, “The Role of Sodium in Aluminum Electrolysis: A possible indicator of cell performance”, Light Metals 1996, pp.319-326.

[19] W. E. Haupin, Principles of Aluminum Electrolysis, *Light Metals 1995, pp.* 195-203

[20] R. Ødegård, Å. Sterten and J. Thonstad, “On the solubility of aluminum in cryolitic melts. Metallurgical Transactions B”, 19(3), pp. 449-457, 1988.

[21] Q. Zhuxian, F. Liman, K. Grjotheim, and H. Kvande, “Formation of Metal Fog during Molten salt Electrolysis Observed in a See-Through Cell”, J. of App. Electrochem., 17(4), pp. 707-714, 1987

[22] T. Støre, “Electrodeposition of Metals from Molten Salts”, Ph.D. dissertation, Norwegian University of Science and Technology, Trondheim, Norway, 1999

[23] G. M. Haarberg, K. S Osen, J. Thonstad, R. J Heus and J. J. Egan, "Measurement of Electronic Conduction in Cryolite Alumina Melts and Estimation of its Effect on Curent Efficiency", Light Metals 1991, pp. 283-281 .

[24] G. M. Haarberg, K. S Osen, J. Thonstad, R. J Heus and J. J. Egan, "Measurement of Electronic Conduction in Cryolite Aiumina Melts and Estimation of its Effect on Current Efficiency", Metallurgical Transactions B, 248, pp. 129-135, 1993

[25] G. M. Haarberg, J. Thonstad, J. J. Egan, R. Oblakowski, and S. Pietrzyk, "Electrical Conductivity Measurements in Cryolite Alumina Melts in the Presence of Aluminium", Light Metals 1996, pp. 221-225.

[26] M. M. Hyland, “The Current Efficiency of a Shorted Anode in a Prebake Cell”,in Journal of Metals, Vol. 35, No. 12, pp. 95-95, 1983

[27] K. Grjotheim, “Nature and Origin of Impurities in the Hall-Héroult Electrolyte and Their Effect on Metal Purity”, International Seminar on Refining and Alloying of Liquid Aluminium and Ferro-Alloys, 1985.

[28] H.A. Øye, “Impurities in Aluminium Smelting”, 5th Australian-Asian Aluminium Smelter Technology Workshop, 1995, pp. 660-680.

[29] Industrial data from Alcoa Fjarðáal, Anode Core Samples, 2012-2014.

[30] E. Haugland, G.M. Haarberg, E. Thisted, J. Thonstad, “The Behaviour of Phosphorus Impurities in Aluminium Electrolysis Cells”, Light Metals 2001, pp. 549-553.

[31] V. Daněk, M. Chrenková, A. Silný, G. M. Haarberg and M. Staš, “Distribution of Phosphorus in Industrial Aluminium Cells”, Canadian Metallurgical Quarterly, 38(3), pp. 149-156, 1999.

[32] L. P. Lossius, H. A. Øye, "Removing Impurities from Secondary Alumina Fines", Light Metals 1992, pp. 249-258.

[33] J. J. del Campo, "La Electrolisis de la Alumina en la Criolita Fundida", PhD dissertation, Universidad de Oviedo, Escuela Tecnica Superior de Ingenieros de Minas, Oviedo, Spain, 1984.

[34] D. Bratland, H. Kvande, W.Q. Bin, "Ionic Species in Cryolite-Sodium Pyrophosphate Melts", Acta Chem. Scand. A41, 377-380, 1987.

[35] M. Chrenková, V. Daněk, A. Silný, "Reactions of Phosphorus in Molten Cryolite", X. Slovak-Norwegian Symposium on Aluminium Smelting Technology, Stará Lesná-Ziar nad Hvonom, Slovakia, Sep. 21-23, 1999.

[36] E. W. Thisted, G. M., Haarberg, and J. Thonstad, "Solubility of $AlPO_4$ in Cryolite melts", Thermochimica acta, 447(1), pp.41-44, 2006.

[37] M. Kucharík and R. Vasiljev, "Solubility of $AlPO_4$ and $NaVO_3$ in $NaF- AlF_3$ Melts", J. of Chem. & Eng. Data, 53(8), 1817-1819, 2008

[38] K. B. Chaudhuri, "Beeinflussung der Aluminiumverluste in Kryolith-Tonerde-Schmelzen durch Badverunreinigungen und Badzusätze", Ph.D. dissertation, Technical University in Berlin, 1968.

[39] J. E. Hatch, "Aluminium – Properties and Physical Metallurgy", American Society for Metals, Chapter 6, pp. 235-236, 1984.

[40] R. E. Frankenfeldt, U. Mannweiler, "Correlation between Pot Gas Collection Efficiency and Metal Purity", 104th AIME annual meeting, 1975, pp. 1-13.

[41] H. Albers, H. C. Wrigge, "The Effect of Reduced Emissions on Aluminum Electrolysis Process", 8th International Congress of ICSOBA, 1997, pp. 485-492.

[42] R. Oblakowski, S. Pietrzyk, "Superheating of Na_3AlF_6-AlF_3-Al_2O_3 Electrolyte in the Process of Aluminium Electrolysis", Metallurgy and Foundry Engineering, 21(3), pp. 175-183, 1995.

[43] E. Böhm, L. Reh, V. Sparwald, G. Winkhaus, "Removal of Impurities in Aluminium Smelter dry gas cleaning using the VAW/Lurgi process", Light Metals 1976, pp. 509-521.

[44] D. R. Augood, "Impurities Distributions in Alumina Reduction Plants", Light Metals 1980, pp. 413-427.

[45] L. Schuh, G. Wedde, "Removal of Impurities from Dry Scrubbed Fluoride Enriched Alumina", Light Metals 1986, pp. 399-403.

[46] E. R. Cutshall, "Removal of Phosphorus from Dry Scrubber Alumina", Light Metals 1979, pp. 927-933.

[47] H. J. Ducote, U.S. Patent No. 4,062,696. Washington, DC, 1977.

[48] L. C. B. Martins, "Use of Dry Scrubber Primary Cyclone to Improve the Purity of Aluminium", Light Metals 1987, pp. 315-317.

[49] E. B. Frolova, V. B. Dobrokhotov, A. M. Tsyplakov, "Effect of Phosphorus Pentoxide on Aluminium Electrolysis", Trudy Vami, N 89, pp. 36-39, 1974.

[50] A. Kerouanton, J. Badoz-Lambling, "Comportment Chimique et Electrochimique de Composes du Phosphore dans la Cryolithe Fondue, Revue de Chimie Minerale", 11, p. 223, 1974.

[51] G. Charlot, J. Badoz-Lambling, P. Homsi, V. Plichon, "Electrochimie dans les Melanges NaF + AlF_3 Fondus", J. Electroanal. Chem., **75**, pp. 665-675, 1977.

[52] M. Keppert, "Electrochemical Behavior of Phosphorus Species in Fluoride Melts", ", Ph.D. dissertation, Norwegian University of Science and Technology, Trondheim, Norway, 2006.

[53] J. B. Metson, and M. M. Hyland, "Sulfur in Anodes-Future Issues and Challenges", 7th Australasian Aluminium Smelting Technology Conference and Workshops, 2001, pp. 233-236.

[54] K. Grjotheim and H. Kvande, "Introduction to Aluminium Electrolysis 2nd ed., Aluminium-Verlag, 1993.

[55] S. J. Hay, "The Formation and Fate of Carbonyl Sulfide (COS) Gas in Aluminium Smelting", PhD dissertation, The University of Auckland, 2002.

[56] J. M. Hunt, "Petroleum Geochemistry and Geology", 2nd ed., New York: W. H. Freeman and Co. 1996.

[57] S. J. Hay, J. B. Metson and M. M. Hyland, "Sulfur Speciation in Aluminum Smelting Anodes", Indust. & Eng. Chem. Research, 43(7), pp. 1690-1700, 2004.

[58] J. B. Metson, S. J. Hay, H. J. Trodahl, B. Ruck and Y. Hu, "The Use of the X-ray Absorption Near Edge Spectrum in Materials Characterization", Current Applied Physics, 4(2), pp. 233-236, 2004.

[59] C. L. Chou, "Geologic Factors Affecting the Abundance, Distribution, and Speciation of Sulfur in Coals", Geology of Fossil Fuels, Proc 30th Int. Geol. Congress, 1997.

[60] R. M. Davidson, "Quantifying Organic Sulfur in Coal: A review", Fuel, 73(7), pp. 988-1005, 1994.

[61] C. L. Spiro, J. Wong, F. W. Lytle, R. B. Greegor, D. H. Maylotte and S. H. Lamson, "X-ray Absorption Spectroscopic Investigation of Sulfur Sites in Coal: Organic Sulfur Identification", Science, 226(4670), pp. 48-50, 1984.

[62] E. Barillon and J. Pinoir, "Use of High-Sulphur Cokes in the Production of Prebake Anodes", Light Metals 1977, pp. 289-299.

[63] E. Barillon, "Evolution Thermique de la Texture Poreuse des Cokes de Petrole", Carbon, Vol 5, pp. 167-171, 1967.

[64] E. Barillon, "Modification de la Texture du Coke de Petrole Lors D'une Désulfuration thermique", J. Chimie Physique, 65, n3, pp. 428, 1968.

[65] E. Barillon, "Evolution Thermique de la Texture du Coke de Brai", J. Chimie Physique, 66, n1, p. 5, 1969.

[66] S. S. Jones, R. D. Hildebrandt, and M. C. Hedlund, Influence of High-Sulfur Cokes on Anode Performance in Alumina Reduction, JOM, 31(9), pp. 33-40, 1979.

[67] V. V. Burnakin, P. V. Polyakov, V. I. Zalivnoy, R. K. Popkova, and V. M. Mozhayev, "Behaviour of Sulfate Ion in Cryolite-Alumina Melts", Sov. J. Non-Ferrous Met. Res., 10, pp. 279-285. 1982.

[68] K. Grjotheim, T. Halvorsen, and S. Urnes, "The Phase Diagram of the System Na_3AlF_6-Na_2SO_4", Can. J. of Chem., 37, pp. 1170-1175. 1959.

[69] I. Koštenská and M. Malinovský, "Phase Diagram of the System NaF—Na_2SO_4", Chem. Zvesti, 36, pp. 159-167, 1982.

[70] V. Danielik, J. Gabčová, "Phase Diagram of the System Na_3AlF_6-NaF-Na_2SO_4", Thermochimica Acta 366, pp. 79-87, 2001.

[71] P. Fellner, J. Gabčová, V. Danielik and M. Laska, "Phase Diagrams of the Ternary System Na_3AlF_6-Na_3FSO_4-Na_2SO_4 and its Thermodynamic Analysis", Chem. Papers 47, 4, pp. 215-217, 1993.

[72] K. Matiašovský and M. Malinovský, Chem. Zvesti, 19, pp. 41-45, 1965.

[73] J. Hajasova, "Electrochemical Behaviour of Sulphur Containing Species in Molten Salts", PhD dissertation, Norwegian University of Science and Technology, Trondheim, Norway, 2007.

[74] A. Nel, "Air Pollution-Related Illness: Effects of Particles", Science 308, N 5723, pp. 804-806, 2005.

[75] P. J. Crutzen, "Albedo Enhancement by Stratospheric Sulfur Injections: a Contribution to Resolve a Policy Dilemma?", Climatic change, 77(3), 211-220, 2006.

[76] K. Tveito, J. Tonheim, K. A. Paulsen and J. Thonstad, "Carbonyl Sulphide (COS) Emissions from Prebake Aluminium Cells", in Greenhouse Gases in the Metallurgical Industries: Policies, Abatement and Treatment Ashfield at the 40th Annual Conference of Metallurgists of CIM (COM 2001), pp. 291-301.

[77] I. Utne, K. A. Paulsen, and J. Thonstad, "The Emission of Carbonyl Sulphide from Prebake and Soderberg Aluminium Cells", Light Metals 1998, pp. 293-301.

[78] F. M. Kimmerle, L. Noël, J. T. Pisano, and G. I. Mackay, "COS, CS_2 and SO_2 Emissions from Prebaked Hall Héroult cells", Light Metals 1997, pp. 153-158.

[79] J. Harnisch, R. Borchers, and P. Fabian, "COS, CS_2 and SO_2 in Aluminium Smelter Exhaust", Environmental Science and Pollution Research, 2(4), pp. 229-232, 1995.

[80] J. L Henry and R. D. Holliday, "Mass Spectrometric Examination of Anode Gases from Aluminium Reduction Cells", JOM, pp.1384-1385, 1957.

[81] R. Oedegard, S. Roenning, A. Sterten, and J. Thonstad, "Sulphur Containing Compounds in the Anode Gas from Aluminium Cells", a Laboratory Investigation, Light Metals 1985, pp. 661-670.

[82] M. M. R. Dorreen, D. L. Chin, J. K. C. Lee, M. M. Hyland, and B. J. Welch, "Sulfur and Fluorine Containing Anode Gases Produced during Normal Electrolysis and Approaching an Anode Effect", Light Metals 1998, pp. 311-316.

[83] V. V. Burnakin, V. I. Zalivnoy, P. V. Polyakov Arskaya L. P and I. Bagaev, "Study of Electrochemical Behavior of Carbon Anodes under Conditions Involving the Use of High Sulfur Coke in the Aluminium Industry", Sov. J. Non-Ferrous Met., 6, pp. 57-58, 1979.

[84] R. J. Thorne et al., "Electrochemical Characterization of Carbon Anode Performance", Light Metals 2013, pp. 1207-1211.

[85] R. J. Thorne et al., “Understanding Anode Overpotential”, Light Metals 2014, pp. 1213-1217.

[86] V. V. Burnakin, L. P. Arskaya, V. I. Zalivnoy, P. V. Polyakov, and V. F. Ofitserov, “The Use of High-Sulfur Cokes in the Production of Anode Paste”, Sov. J. Non-Ferrous Met. 6, pp. 68-70, 1981.

[87] V. V. Burnakin, R. K. Popkova, V. I. Zalivnoy, P. V. Polyakov and V. I. Kolosova, “Behaviour of Sulfate Ion during the Electrolysis of Aluminium”, Sov. J. Non-Ferrous Met. Res., 2, (4), pp. 282-285, 1983.

[88] Y. V. Baimakov and M. M. Vetyukov, “Electrolysis of Fused Salts Metallurgiya”, Moscow, 1966, pp. 410-412.

[89] P. Fellner, M. Korenko, M. Ambrová, V. Danielik, and J. Thonstad, “Reactions of Sulphides in Molten Cryolite”, Thermochimica Acta, 410(1), pp. 87-91, 2004.

[90] P. Fellner, M. Ambrová, J. Híveš, M. Korenko and J. Thonstad, “Chemical and Electrochemical Reactions of Sulphur Species in Cryolite Melts”, Light Metals 2005, pp.577-581.

[91] M. Ambrová, P. Fellner, J. Gabcova, and A. Sykorova, “Chemical Reactions of Sulphur Species in Cryolite-Based Melts, Chemical Papers-Slovak Academy of Sceinces, 59(4), pp. 235, 2005.

[92] M. Ambrová, P. Fellner, and J. Thonstad, “Anodic Reactions of Sulphate in Molten Salts”, Chemical Papers, 64(1), pp. 8-14, 2010.

[93] M. Ambrová, P. Fellner, J. Jurišová and J. Thonstad, “Electrode Processes of Sulphur Species in Molten Salts”, Light Metals 2007, pp. 363-368.

[94] M. Ambrová, V. Danielik, P. Fellner and J. Thonstad, “The Cathode Process in Sodium Chloride Melts Containing Sulphate”, Electrochimica Acta, 51(26), pp. 5825-5828, 2006.

[95] M. A. Castro, K. Faulds, W. E. Smith, A. J. Aller and D. Littlejohn, “Identification of Condensed-Phase Species on the Thermal Transformation of Alkaline and Alkaline Earth Metal Sulfates on a Graphite Platform”, Spectrochimica Acta Part B, 59, pp. 827-839, 2004.

[96] G. J. Houston, and H. A. Øye, “Carbon Losses Caused by Gaseous Oxidation during Aluminium Electrolysis”, Aluminium 61, pp. 250-254, 346-349, 426-428, 1985.

[97] T. Eidet, M. Sørlie and J. Thonstad, “Effects of Sulphur, Nickel and Vanadium on the Air and CO_2 Reactivity of the Cokes”, Light Metals 1997, pp. 436-437.

[98] M. Aanvik, M. Sørlie and H. A. Øye, “Reactivity and texture of cokes doped with aluminium compounds” Light Metals 2000, pp. 555-561.

[99] Y. D. Bensah and T. Foosnaes, “The Nature and Effect of Sulphur Compounds on CO_2 and Air Reactivity of Petrol Coke”, J. of Eng. & App. Sc., 5(6), pp. 35-43, 2010.

[100] J. Xiao, Q. Zhong, F. Li, J. Huang, Y. Zhang and B. Wang, “Mutual Inhibition between Catalytic Impurities of Sulfur and Those of Calcium in Coke during Carbon–Air and Carbon–CO_2 Reactions”, Energy & Fuels, 29(3), pp. 1961-1971, 2015.

[101] J. Xiao, S. Y. Deng, Q. F. Zhong and S. L. Ye, "Effect of Sulfur Impurity on Coke Reactivity and its Mechanism", Transactions of Nonferrous Metals Society of China", 24(11), pp. 3702-3709, 2014.

[102] K. Khaji and M. Qassemi, "Factors Influencing Baked Anode Properties", Light Metals 2015, pp.1135-1140.

[103] V. L. Bullough, H. C. Marshall, and C. J. McMinn, "Some Effects of Sulfur in Petroleum Coke on the Performance of Anodes in Prebake Alumina Reduction Cells", Light Metals 1971, 134, pp. 411-423.

[104] T. G. Pearson, "The Chemical Background of the Aluminium Industry, Royal Institute of Chemistry", Lectures, Monographs and Reports, N 3, pp.43, 1955.

[105] A. F. LaCamera, S. P. Ray, X. Liu, R. L. Kozarek and J. L. Roddy, U.S. Patent No. 6,866,766. Washington, DC: U.S. Patent and Trademark Office, 2005.

[106] R. Meirbekova, G.M. Haarberg, J. Thonstad, D. P. Ziegler, J. Brynjarsson and G. Saevarsdottir, "Effect of Operatinal Parameters on the Behavior of Phosphorus and Sulfur in Aluminum Reduction", Light Metals 2015.

[107] S. Rolseth, T. Muftuoglu, A. Solheim, J. Thonstad, "Current Efficiency at Short Anode-Cathode Distance in Aluminum Electrolysis", *Light Metals 1986*, pp. 517-523.

[108] P. N. Booth et al, "Risk Assessment as a Decision-Making Tool for Treatment of Emissions at a New Aluminum Smelter in Iceland: 1. Background and introduction", Human and Ecological Risk Assessment, 15(3), pp. 423-441, (2009).

[109] S. Rolseth, Tilbakereaksjonen i Aluminiumelektrolysen, Ph.D. dissertation, Norwegian University of Science and Technology, Trondheim, Norway 1980.

[110] J. P. Armoo, The Current Efficiency for Aluminum Deposition from Cryolte Alumina Melts at High Current Density, M.S. thesis, NTNU, Trondheim, Norway 2010.

[111] P. V. Polyakov, V. Y. Buzunov, Y. G. Mikhaev and V. G. Printsev, Movement of Metal-Electrolyte Interface in Aluminum Reduction Cells by Marangani Effect, Tsvetnye Metally, 34, N 3, pp. 29-31, 1993.

[112] W.Haupin and W. McGreew, Aluminium 51, 273, 1975.

[113] Å. Sterten, "Current Efficiency in Aluminium Reduction Cells", J. of App. Electrochem., 18(3), pp. 473-483, 1988.

[114] P. A. Solli, E. Skybakmoen, and Å. Sterten, "Current Efficiency in the Hall-Héroult Process for Aluminum Electrolysis: Experimental and Modeling Studies", J. Appl. Electrochem., 27, pp. 939-946, 1997.

[115] R. Meirbekova, G. M. Haarberg, J. Thonstad and G. Saevarsdottir, "Influence of Sulfur Species on Current Efficiency in the Aluminum Smelting Process", submitted for publication.

[116] A. Solheim, private communication.

[117] N. Q. Minh, and N. P. Yao, "The Anodic Reaction of Sulfide Ions at Graphite Electrodes in Molten Cryolite", J. of Electrochem. Soc., 131(10), pp. 2279-2282, 1984.

[118] R. Meirbekova, G. M. Haarberg, T. A. Aahaug, J. Thonstad, and G. Saevarsdottir, “Behavior of Sodium Sulfate in Cryolite-Alumina Melts and the Formation of Sulfurous Gases”, submitted for publication.

[119] M. Ambrová, J. Jurišová, P. Fellner and Thonstad, J., “Determination of Sulphur Species in Solidified Cryolite Melts”, Chemical Papers, 66(7), pp.621-625, 2012.

SUPPLEMENT 1

R. Meirbekova, G.M. Haarberg and, G. Saevarsdottir, Effect of Phosphorus Impurities on the Current Efficiency for Aluminum Deposition from Cryolite-Alumina Melts in a Laboratory Cell, in Molten Salts Chemistry and Technology, John Wiley & Sons, pp.71-75.

The layout and text size have been changed to improve readability.

SUPPLEMENT 2

R. Meirbekova, G. Saevarsdottir, G.M. Haarberg and J.P. Armoo, "Effect of Current Density and Phosphorus Impurities on the Current Efficiency for Aluminum Deposition in Cryolite-Alumina Melts in a Laboratory Cell", Light Metals 2013, pp.917-920.

The layout and text size have been changed to improve readability.

SUPPLEMENT 3

R. Meirbekova, J. Thonstad, G.M. Haarberg and G. Saevarsdottir, "Effect of Current Density and Phosphorus Species on Current Efficiency in Aluminium Electrolysis at High Current Densities", Light Metals 2014, pp.759-764.

The layout and text size have been changed to improve readability.

SUPPLEMENT 4

R. Meirbekova, G.M. Haarberg, J. Thonstad, Donald P. Ziegler, J. Brynjarsson and G. Saevarsdottir, "Effect of Operational Parameters on the Behaviour of Phosphorus and Sulfur on Aluminium Reduction", Light Metals 2015, pp.559-564.

The layout and text size have been changed to improve readability.

SUPPLEMENT 5

R. Meirbekova, G.M. Haarberg, J. Thonstad, and G. Saevarsdottir, Influence of Sulfur Species on Current Efficiency in the Aluminum Smelting Process, submitted to Metallurgical and Material Transactions B.

The layout and text size have been changed to improve readability.

SUPPLEMENT 6

R. Meirbekova, G.M. Haarberg, J. Thonstad, T. A. Aahaug and G. Saevarsdottir, "Behavior of Sodium Sulfate in Cryolite-Alumina Melts and Formation of Sulfurous Gases", submitted to ECS Transactions.

The layout and text size have been changed to improve readability.